Table 1. Surface marker analysis of the NOD/SCID repopulating ATL-like lymphoma cells

Phenotype	Frequency (%)
$CD38^-/CD71^-/CD117^+$	0.03-0.05
$CD38^-/CD71^-/CD133^+$	0
$CD38^-/CD71^-$	0.3-0.5
$CD38^-/CD117^+$	0.10
$CD71^-/CD117^+$	0.15
$CD38^-/CD133^+$	< 0.01
$CD71^-/CD133^+$	< 0.01
Side population cells*	0.03-0.06
Aldehyde dehydrogenase activity*	0

Summary of surface marker combination analysis of ATL-like lymphoma cells in the NOD/SCID mouse. $CD38^-/CD71^-/CD117^+$ cells were overlapped with side population cells.

*Functional assay.

weight was significantly increased only in the CSC-transplanted-NOD/SCID mouse spleen (Figure 4D). No lymphoma was observed after transplantation of 10^2 SLCs (n = 11) and the non-CSC fraction ($CD38^+/CD71^+/CD117^-$; n = 11) at 60 days. Analysis of the splenic cells isolated from 10^2 CSC-transplanted NOD/SCID mouse showed similar profiles to the first transplantation experiment using 10^5 SLCs, in that they were $CD25^+/CD44^+$ (data not shown) and contained SP cells (0.06%; Figure 4E) and the CSC-associated ($CD38^-/CD71^-/CD117^+$) cell population (Figure 4F). These results clearly show that within this cell population are CSCs in that they have the SP phenotype and have the potential for self-renewal and the ability to regenerate the original lymphoma and leukemia.

Histologic analysis of spleen, BM, and other tissues

To confirm and characterize in more detail the lymphoma and leukemia in spleen after transplantation with the candidate CSCs,

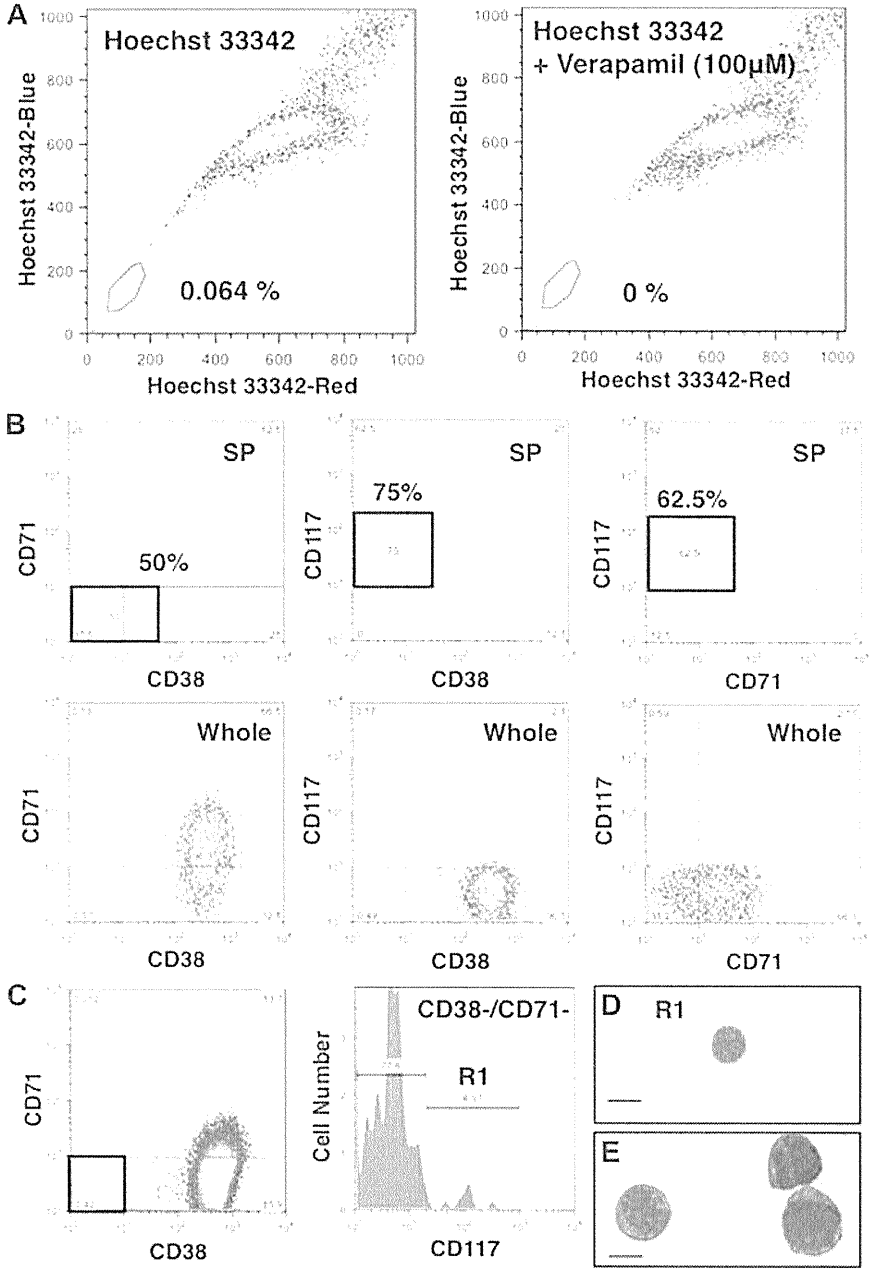

Figure 3. Functional analysis in the NOD/SCID repopulating ATL-like lymphoma cells. (A) SP cell analysis in the NOD/SCID repopulating ATL-like lymphoma cells. The SP regions are indicated by a trapezoid on each panel. (Left panel) Approximately 0.064% of SP cells were observed in the SLCs. (Right panel) SP cell analysis after treatment with verapamil (100 μM), where the SP fraction was lost. (B) Triple-staining analysis of CD38, CD71, and CD117 in the SP fraction. More than 50% of $CD38^-/CD71^-/CD117^+$ corresponded to the SP fraction. (C) FACS $CD38^-/CD71^-/CD117^+$ and $CD38^-/CD71^-/CD117^-$ cells. (D) Cytospin analysis of the CSC candidate ($CD38^-/CD71^-/CD117^+$) and (E) non-CSC candidate ($CD38^+/CD71^+/CD117^-$) populations.

Table 2. Limiting dilution analysis in assessing stem cell activity

No. of cells	SLCs	CSCs ($CD38^-/CD71^-/CD117^+$)	Non-CSCs ($CD38^+/CD71^+/CD117^-$)
Short-term incubation (40 days)			
10^6	5/5	NT	NT
10^5	3/4	NT	NT
10^4	3/3	NT	NT
10^3	1/5	NT	NT
10^2	0/7	0/6	NT
Long-term incubation (60 days)			
10^2	0/11	9/9	0/11

Assessment of stem cell activity in the ATL-like lymphoma cell using limiting dilution assay of transplantation cells. One CSC was thought to exist in 10^4 SLCs. At long-term incubation, only CSC fractions can repopulate and regenerate original ATL-like lymphoma in the NOD/SCID mouse.

NT indicates no transplantation.

we performed histologic and immunohistochemical analyses. It has been reported that ATL leukemic cells have abundant PAS-strong positive cytoplasmic inclusions.[18] We could show that PAS-hematoxylin strong positive staining was only observed in lymphoma and leukemia in spleens after transplantation with 10^5 SLCs and 10^2 CSCs (Figure 5A-B). PAS-strong positive cells were not identified in the spleen after transplantation with 10^2 non-CSCs and SLCs (Figure 5C). To confirm the existence of malignant cells, we performed immunohistochemistry for CD3, CD4, CD44, and CD117. $CD3^+$ leukemic cells were observed only in the splenic lymphoma after transplantation of 10^2 CSCs and 10^5 SLCs. No $CD4^+$ cells were observed in the CSCs and non-CSC–transplanted

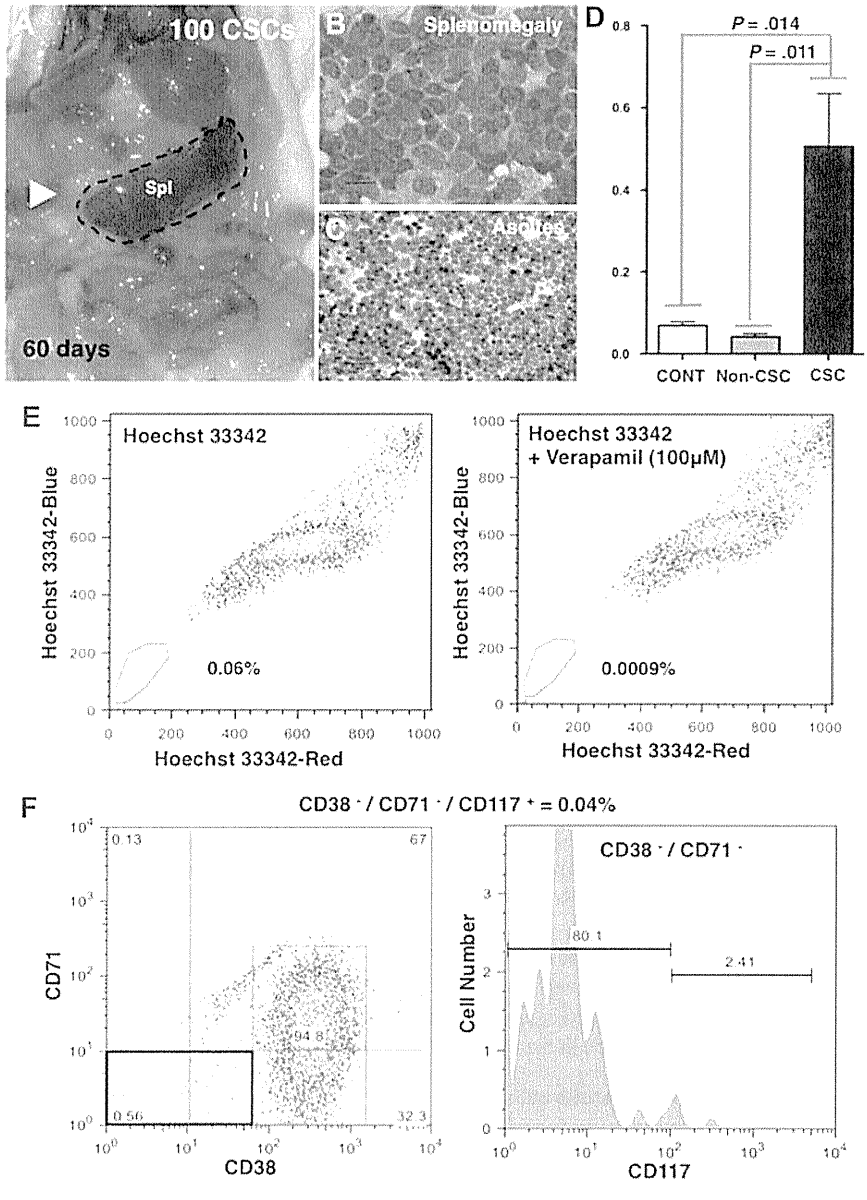

Figure 4. Regenerative potential of ATL-like lymphoma in 10^2 CSCs. ATL-like lymphoma-regenerative activity was assessed by the transplantation of 10^2 CSCs, the non-CSC fraction, and SLCs. (A) ATL-like lymphoma was regenerated by the transplantation of 10^2 CSCs into the NOD/SCID mouse at 60 days. (B) Marked splenomegaly was observed in the NOD/SCID recipient mice. (C) Ascites was also observed in the NOD/SCID recipient mice. (D) Total spleen weight was significantly increased only in the CSC-transplanted NOD/SCID mouse. (E) SP analysis of ATL-like lymphoma cells generated by the transplantation of 10^2 CSCs. (Left panel) The SP fraction (total = 0.066%) was present after CSC transplantation. (Right panel) The SP fraction was lost in the dot plot with treatment by 100 μM verapamil. (F) Surface marker analysis in the lymphoma cells regenerated by the 10^2 CSC transplantation. The CSC candidate cells ($CD38^-/CD71^-/CD117^+$) were also regenerated after transplantation of 10^2 CSCs.

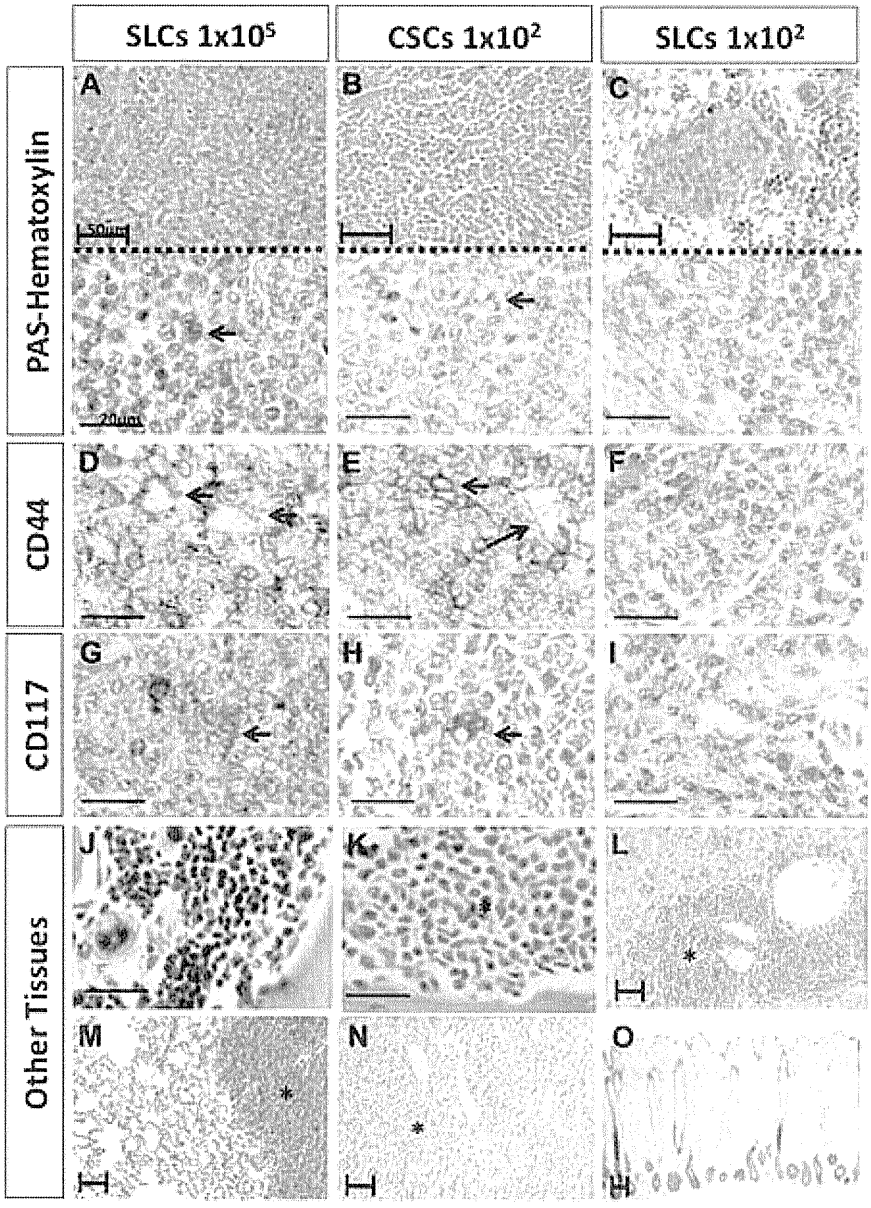

Figure 5. Histologic and immunohistochemical analyses of spleen after transplantation. At 60 days, lymphoma was regenerated after the transplantation of 10^5 SLCs and 10^2 CSCs. No lymphoma was observed after the transplantation of 10^2 non-CSCs. (A) PAS-hematoxylin staining in the 10^5 SLCs recipient spleen. (Top panel) Low magnification. (Bottom panel) High magnification. Strong PAS^+-stained cells were observed (↔). (B) PAS-hematoxylin staining in the 1×10^2 CSCs recipient spleen. (C) PAS-hematoxylin staining in the 1×10^2 non-CSCs recipient spleen. No strong PAS^+ staining cells were evident. (D-I) Immunohistochemistry of CD44 and CD117, shown in the 10^5 SLC recipient spleen (D,G), in the 10^2 CSC recipient spleen (E,H), and in the 1×10^2 SLC recipient spleen (F,I). CD44 and CD117 expression is detected in the lymphoma in the spleen after 1×10^5 SLC and 1×10^2 CSC transplantation. (J) Hematoxylin and eosin (H&E) staining of the normal NOD/SCID mouse BM. Various types of blood cells, including megakaryocytes and erythroid cells, were evident. (K) Hematoxylin and eosin staining of lymphoma reconstituted in the NOD/SCID mouse BM. The BM tissue was uniformly filled with ATL-like lymphomatous cells. (L) Infiltration of lymphomatous cells was also observed in the liver. (M) Infiltration of lymphomatous cells in lung. (N) Infiltration of lymphomatous cells in lymph nodes. (O) Infiltration of lymphomatous cells was not observed in the epidermal tissues. *Lymphomatous cells. (Closed scale bar, 50 μm; open scale bar, 20 μm.)

spleen (data not shown). Interestingly, CD44 strongly positive cells were identified only in the lymphomatous spleen (Figure 5D-E) and not in the nonlymphomatous spleen (Figure 5F). Moreover, $CD117^+$ cells serving as a surrogate CSC marker were identified only in the lymphomatous spleen (Figure 5G-H) and not in the nonlymphomatous spleen (Figure 5I).

To confirm the infiltration of lymphomatous cells in other tissues, we next performed histologic analysis on BM, liver, lung, lymph node, and epidermal tissues. In the BM, as expected, various types of blood cells, including megakaryocytes and erythroid cells, were observed in WT NOD/SCID BM (Figure 5J). However, ATL-like lymphomatous cells uniformly filled in the BM of transplanted animals (Figure 5K). In addition to the BM, lymphomatous cells were also observed in the liver (Figure 5L), lung (Figure 5M), and lymph node (Figure 5N). Infiltration of lymphomatous cells was not observed in the epidermal tissues (Figure 5O).

Identification of lymphomatous cells in BM

We performed cell surface analysis of the BM mononuclear cells isolated from NOD/SCID mouse, after transplantation with 10^5 SLCs. $CD38^-/CD71^-/CD117^+$ cells (0.05%) could also be detected in BM (Figure 6A). Although, in the normal NOD/SCID mouse BM, $CD3^+$ cells were rare (Figure 6B), in contrast, almost all cells in the transplanted NOD/SCID mice were $CD3^+$ (Figure 6C).

In normal hematopoiesis, HSCs are located in specific microenvironments (niches) that also play a role in maintaining stem cell function. The osteoblastic niche in the trabecular bone and vascular niche in the medullary region are important for both the maintenance of hematopoietic[20] and leukemic stem cell function. To identify the niches of the CSCs in the BM, we performed CD117 staining as a surrogate CSC marker. Notably, $CD117^+$ cells were located both in the osteoblastic niche region (Figure 6D) in the trabecular bone and vascular niche in the medullary region (Figure 6E).

Molecular characterization and Tax expression in CSCs

To identify specific molecular markers in CSCs, we performed real-time PCR analysis on isolated CSC and non-CSC fractions (Figure 7). Recently, several molecules have been indentified as

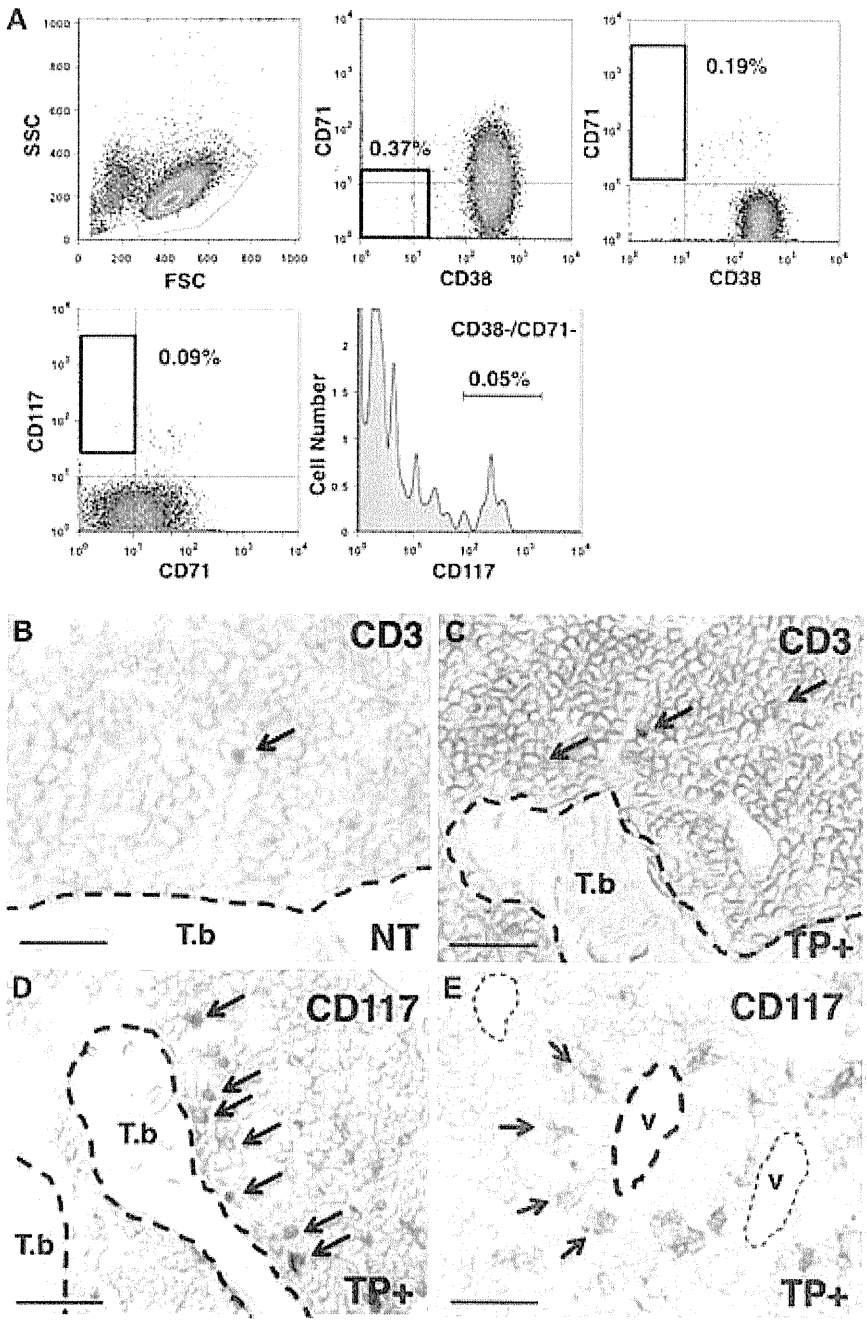

Figure 6. Flow cytometric analysis of lymphomatous cells in the NOD/SCID BM. NOD/SCID repopulating lymphomatous cells were isolated from BM. (A) Triple staining analysis with CD38, CD71, and CD117 in the BM SLCs. As was observed in spleen, the CSC candidates were also observed in the BM. (B) Histologic analysis of ATL-like lymphomatous cells in the NOD/SCID BM. In the normal NOD/SCID BM, $CD3^+$ cells were a rare population (←). (C) In the reconstituted NOD/SCID mouse BM, $CD3^+$ cells were readily identified (arrow). (D) $CD117^+$ cells as a surrogate CSC marker could be detected in the osteoblastic niche of the trabecular bone (arrow). (E) In the medullary region, $CD117^+$ cells (CSCs) were also detected in the vascular niche (←). T.b. indicates endosteal region in the trabecular bone; V, vascular zone; TP+, transplantation; and NT, no transplantation. Scale bar represents 20 μm.

being associated with tumor progression. Several embryonic stem cell markers have been shown to be associated with osteosarcoma[30] and bladder cancer,[31] and several HSC markers were found to be associated with leukemia development.[32] We examined *Notch1*, *CD44*, *Oct-4*, *Nanog*, *Rex1*, *Bmi1*, *SCL/tal-1*, *Flt3*, *N-cadherin*, and viral *Tax* expression in the CSCs. A total of 5×10^3 CSCs and non-CSCs were isolated by fluorescence-activated cell sorter (FACS) for RNA isolation and cDNA synthesis. These amplified cDNA were initially validated by *CD117* expression (Figure 6A). The expression level of *CD117* in the CSCs was higher than in the non-CSC fraction. In contrast, expression of *HTLV-1 Tax* mRNA was extremely low compared with the non-CSC fraction. Although expression of *CD44* in the CSC was higher than in the non-CSC fraction, *Notch1* and *Bmi-1* expression was lower than in the non-CSCs (Figure 6B). No differences were observed in *Rex1*, *Flt3*, *SCL/tal-1*, *N-cadherin*, *Oct-4*, and *Nanog* expression (data not shown).

Discussion

In this study, we have successfully identified a candidate CSC population in a mouse model of ATL, which has been shown to exhibit many of the clinical, pathologic, and immunologic features of human disease. It has been clearly established that CSCs are a specific and minor cell population, which have the potential for self-renewal, differentiation, aggressive proliferation, and chemotherapy resistance and can successfully regenerate the original malignancy when transplanted into immunocompromised mice.[14] In hematologic malignancies, several CSC candidates have been identified in acute myeloid leukemia,[12] chronic myeloid leukemia,[13] and acute lymphoblastic leukemia (ALL). Recently, Cox et al have characterized different CSC populations in ALL, which

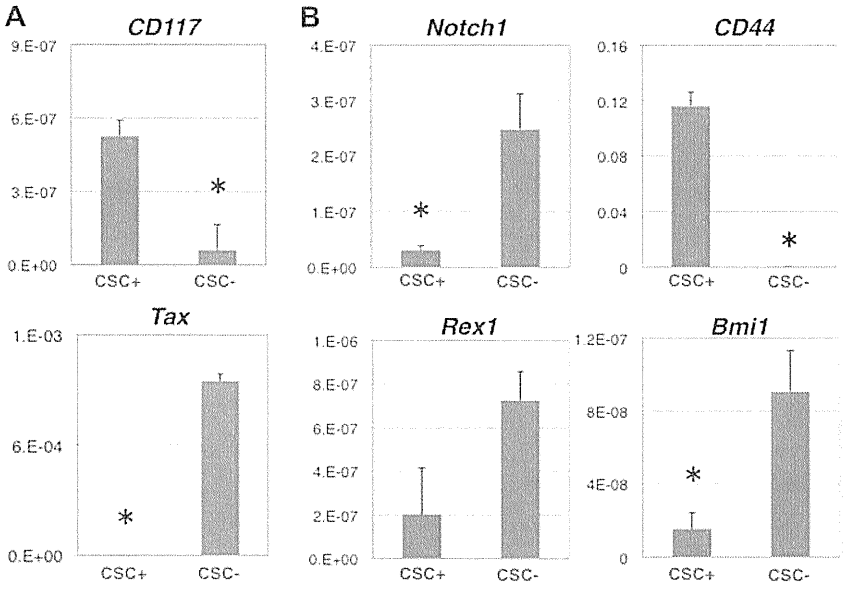

Figure 7. Molecular characterization of the CSCs and non-CSC fraction. FACS-sorted 5000 CSCs and non-CSCs were used to purify RNA and synthesize cDNA. Gene expression level was determined relative to *β-actin*. (A) *CD117* expression was used to evaluate the efficacy of cell sorting. (Top panel) *CD117* expression was higher in the CSCs than in the non-CSCs. (Bottom panel) Tax gene expression was not detected in CSCs. (B) *Notch1* and *Bmi1* expression was down-regulated in CSCs. *CD44* expression was up-regulated in CSCs. No difference was observed in the expression of the other genes, *Rex1*, *Flt3*, *SCL/tal-1*, *N-cadherin*, *Oct-4*, and *Nanog* in the CSCs and non-CSC fraction. *$P < .05$ (significant).

include the phenotype $CD34^+/CD10^-$ or $CD34^+/CD19^-$ subpopulations in B-ALL and $CD34^+/CD4^-$ or $CD34^+/CD7^-$ subpopulations in childhood T-ALL.[33,34] Although it has been suggested that leukemic transformation occurs in a committed T- and B-cell lineage,[35] both of these candidates express the hematopoietic progenitor marker CD34, suggesting that T- and B-cell leukemia may have arisen in an early hematopoietic precursor.

ATL is a lymphoproliferative disorder caused by infection with HTLV-1.[1] Although various chemotherapeutic regimens have provided significant initial complete remission rates, most treated patients relapse, and these observations have suggested the existence of drug-resistance CSCs in aggressive disease. In this study, we have, for the first time, successfully identified and enriched a candidate CSC population in an ATL model mouse using SP analysis in conjunction with cell surface marker identification by flow cytometry. The candidate CSCs identified by their SP phenotype, which were found to overlap with a $CD38^-/CD71^-/CD117^+$ population, could regenerate the original lymphoma/leukemia with the expected phenotype when transplanted in SCID/NOD mice.

Recently, Kayo et al reported the existence of SP cells in several cultured ATL cell lines, which were defined by efficient efflux of Hoechst 33342 dye.[36] However, in these studies, both SP cells and non-SP cells could reconstitute both SP and main population cells, suggesting that SP cells in the cell lines had no specific CSC-like function in vitro.[36] The reasons for this are unclear but may well reflect changes in the cell populations as a result of culture. It has also been reported that CD90 may be a useful marker to identify CSCs in ATL cell lines. CD90 (Thy-1) is a hematopoietic progenitor marker, which is not expressed in mature T cells. In our experiments, CD90 expression was detected in approximately 1.5% of SLCs; however, expression was not associated with the CSCs. These disparate results may again reflect the differences between our transgenic and SCID/NOD animal models and ATL cell lines, which may have changed during culture.

CSCs, especially in the hematologic malignancies, share many properties with HSCs, and indeed almost all CSCs are thought to be derived from HSCs.[32] Although It has been shown that human ATL is a leukemia that, in most cases, is derived from $CD4^+$ mature T cells,[3] others exhibit a phenotype of cells at early stages in T-cell development. In our Tax transgenic mouse model, it has been shown that the ATL-like lymphoma cells were derived from an immature pre-T cell (DN2), which expresses cytoplasmic CD3, and surface CD25 and CD44.[8] In the present study, we could clearly demonstrate that the $CD38^-/CD71^-/CD117^+/CD44^+$ fraction have lymphoma and leukemia-initiating potential and proliferation activity, and have markers expressed in hematopoietic progenitor cells (CLP; common lymphoid progenitor) or Pro-T cells (DN1; double negative). CD117 (also known as c-kit) is useful marker for identifying long-term and short-term repopulating HSCs. Recently, it has shown that CD117 and its ligand stem cell factor also have important roles in early T-cell development,[37] and Notch1 with IL-7 induced differentiation of early progenitors with lymphoid and myeloid properties (EPLM) into T-cell lineage is dependent on CD117 signaling.[38] In addition to CD44, CD117 expression and the SCF/CD117 signaling pathway are also required to initiate the development of several lymphocyte populations.[39] *Notch1* is expressed in long-term HSCs and regulates the self-renewal activity of long-term HSCs in the osteoblastic niche via *Nocth1* receptor ligand *Jagged1*.[40] However, in the T-cell commitment process, whether activation of *Notch1* signaling occurs before or after EPLMs enter the thymus is still controversial.[41] In our experiments, *Notch1* expression in CSCs was down-regulated compared with the non-CSC fraction, suggesting that CSCs were derived from the EPLM or hematopoietic progenitor cells and that activation of Notch1 may be required to induce T-cell lymphoma and leukemia. It has been shown that a mutation (t(7;9) translocation) and constitutive activation of *Notch1* are frequently observed in T-ALL.[42] Whether activation of NOTCH1 signaling and in our animal model or indeed in ATL patients is related to HTLV-1 infection and Tax expression is still unclear and remains to be investigated. However, our data suggest and support the view that, at least in our mouse model, the T-cell lymphoma and leukemia-initiating stem cell is derived from an HTLV-1–infected EPLM or early hematopoietic progenitor cell and suggest that CD44 and CD117, if present, in human ATL CSCs could be possible therapeutic targets for treatment of aggressive disease.

It has been suggested that HTLV-1–derived Tax gene expression plays a key role in the development of ATL and particularly in the early stages of cell proliferation and transformation. Paradoxically, Tax gene expression is either undetectable or only at very low levels in fresh uncultured human ATL cells. In our Tax-transgenic

mouse model, Tax gene expression was also expressed at very low levels only being detected by sensitive reverse-transcription RT-PCR assays. In the present study, we found a significant further down-regulation of Tax gene in the CSCs compared with cells in the non-CSC fraction. These data support our hypothesis that CSCs are derived from EPLM or early pro-T cells (so-called DN1), as the *Lck* promoter will drive partially from DN2 and completely from the DN3 stages.[43] Recent studies have also shown that HTLV-1 can infect HSCs,[6] and lentiviral-mediated expression of Tax gene in human $CD34^+/CD38^-$ cells resulted in G_0/G_1 cell-cycle arrest by P21 and P27 up-regulation and the suppression of multilineage hematopoietic differentiation.[44] These results would suggest that the reacquisition of stem cell properties in T cell–committed progenitors might require both *Tax* expression and *CD117* and *Notch1* reexpression.

In the quantitative real-time PCR analysis, contrary to our expectations, we found a strong down-regulation of *Bmi1* in CSCs, which has been shown to be involved in the progression of several malignancies.[27] Recently, Miyazaki et al[45] reported that *Bmi1* is required for the survival, the activation of pre-T cell, and the transition from DN to double-positive cells. Although expression of *Bmi1* was detected in DN-stage, dependent up-regulation of *Bmi1* was observed from DN2 to DN4.[45] These data support our proposal that the CSCs were derived from EPLMs, but the mechanism of *Bmi1* activation in these cells remains to be investigated.

At present, the microenvironment of CSCs has not been clearly identified. Recently, Ishikawa et al reported that acute myeloid leukemia leukemic stem cells engraft within osteoblastic niche of the BM, and it has been suggested that this may afford protection from chemotherapy-induced apoptosis.[46] In the present study, we have identified potential BM niches for our candidate CSCs in the NOD/SCID model. Specifically, we found that CSCs were located both in the osteoblastic and vascular niches, but further studies are required to determine whether the former localization might also contribute to resistance to chemotherapy in our CSCs, and this is currently under investigation.

In conclusion, our transgenic and NOD/SCID animal studies have allowed the identification of candidate CSCs in this model of ATL. We think that our investigations will both inform and provide a basis for similar studies on human disease to determine whether these or equivalent stem cell populations exist and have the same characteristics. If successful, this will potentially allow the development of new anti-CSC therapeutics, which may provide more effective treatment for human disease.

Acknowledgments

The authors thank Dr Toshiki Watanabe for his critical reading of the manuscript.

This work was supported in part by the Grant-in-Aid for Scientific Research of Ministry of Education, Culture, Sports, Science and Technology, Japan (no.18790669). H.H. was supported by the Japan Society for the Promotion of Science (JSPS; Grants-in-Aid for Scientific Research), the Ministry of Health, Labor and Welfare Japan, and the Takeda Science Foundation.

Authorship

Contribution: J.Y., T.M., and I.H. designed the research; J.Y. performed the majority of FACS and transplantation analysis; T.M. performed the histologic studies, analyzed the data, and wrote the paper; K.T. assisted with cell sorting and transplantation experiments; M.K. performed the quantitative PCR experiments; H.M. and A.M. also performed experiments; Y.A. assisted with the NOD/SCID mouse experiments; H.H. and W.W.H. produced the Tax transgenic mice, developed the NOD/SCID model, and wrote the paper; and H.T. and K.Y. were involved in the design of the research.

Conflict-of-interest disclosure: The authors declare no competing financial interests.

Correspondence: Isao Hamaguchi, Department of Safety Research on Blood and Biological Products, National Institute of Infectious Diseases 4-7-1, Gakuen, Musashimurayama, Tokyo, 208-0011, Japan; e-mail: 130hama@nih.go.jp.

References

1. Yamaguchi K. Human T-lymphotropic virus type I in Japan. *Lancet.* 1994;343(8891):213-216.
2. Proietti FA, Carneiro-Proietti AB, Catalan-Soares BC, Murphy EL. Global epidemiology of HTLV-I infection and associated diseases. *Oncogene.* 2005;24(39):6058-6068.
3. Shimoyama M. Diagnostic criteria and classification of clinical subtypes of adult T-cell leukaemia-lymphoma: a report from the Lymphoma Study Group (1984-87). *Br J Haematol.* 1991;79(3):428-437.
4. Yamada Y, Kamihira S, Amagasaki T, et al. Adult T cell leukemia with atypical surface phenotypes: clinical correlation. *J Clin Oncol.* 1985;3(6):782-788.
5. Karube K, Ohshima K, Tsuchiya T, et al. Expression of FoxP3, a key molecule in CD4CD25 regulatory T cells, in adult T-cell leukaemia/lymphoma cells. *Br J Haematol.* 2004;126(1):81-84.
6. Feuer G, Fraser JK, Zack JA, Lee F, Feuer R, Chen IS. Human T-cell leukemia virus infection of human hematopoietic progenitor cells: maintenance of virus infection during differentiation in vitro and in vivo. *J Virol.* 1996;70(6):4038-4044.
7. Matsuoka M, Jeang KT. Human T-cell leukaemia virus type 1 (HTLV-1) infectivity and cellular transformation. *Nat Rev Cancer.* 2007;7(4):270-280.
8. Hasegawa H, Sawa H, Lewis MJ, et al. Thymus-derived leukemia-lymphoma in mice transgenic for the Tax gene of human T-lymphotropic virus type I. *Nat Med.* 2006;12(4):466-472.
9. Ohsugi T, Kumasaka T, Okada S, Urano T. The Tax protein of HTLV-1 promotes oncogenesis in not only immature T cells but also mature T cells. *Nat Med.* 2007;13(5):527-528.
10. Yamada Y, Tomonaga M, Fukuda H, et al. A new G-CSF-supported combination chemotherapy, LSG15, for adult T-cell leukaemia-lymphoma: Japan Clinical Oncology Group Study 9303. *Br J Haematol.* 2001;113(2):375-382.
11. Mahieux R, Hermine O. In vivo and in vitro treatment of HTLV-1 and HTLV-2 infected cells with arsenic trioxide and interferon-alpha. *Leuk Lymphoma.* 2005;46(3):347-355.
12. Jordan CT. Unique molecular and cellular features of acute myelogenous leukemia stem cells. *Leukemia.* 2002;16(4):559-562.
13. Holyoake TL, Jiang X, Drummond MW, Eaves AC, Eaves CJ. Elucidating critical mechanisms of deregulated stem cell turnover in the chronic phase of chronic myeloid leukemia. *Leukemia.* 2002;16(4):549-558.
14. Al-Hajj M, Clarke MF. Self-renewal and solid tumor stem cells. *Oncogene.* 2004;23(43):7274-7282.
15. Clarke MF. A self-renewal assay for cancer stem cells. *Cancer Chemother Pharmacol.* 2005;56[Suppl 1]:64-68.
16. Tang C, Ang BT, Pervaiz S. Cancer stem cell: target for anti-cancer therapy. *FASEB J.* 2007;21(14):3777-3785.
17. Goodell MA, Brose K, Paradis G, Conner AS, Mulligan RC. Isolation and functional properties of murine hematopoietic stem cells that are replicating in vivo. *J Exp Med.* 1996;183(4):1797-1806.
18. Takemori N, Hirai K, Onodera R, Saito N, Kamiguchi K, Namiki M. Vacuolated glycogen-laden leukemic cells in a case of crisis type chronic adult T-cell leukemia. *Leuk Lymphoma.* 1993;11(3):309-314.
19. Hamaguchi I, Imai J, Momose H, et al. Two vaccine toxicity-related genes Agp and Hpx could prove useful for pertussis vaccine safety control. *Vaccine.* 2007;25(17):3355-3364.

20. Mizukami T, Kuramitsu M, Takizawa K, et al. Identification of transcripts commonly expressed in both hematopoietic and germ-line stem cells. *Stem Cells Dev.* 2008;17(1):67-80.
21. Kohno T, Yamada Y, Akamatsu N, et al. Possible origin of adult T-cell leukemia/lymphoma cells from human T lymphotropic virus type-1-infected regulatory T cells. *Cancer Sci.* 2005;96(8):527-533.
22. Baba H, Yamada Y, Mori N, et al. Multiple gamma-receptor expression in adult T-cell leukemia. *Eur J Haematol.* 2002;68(6):362-369.
23. Bonnet D, Dick JE. Human acute myeloid leukemia is organized as a hierarchy that originates from a primitive hematopoietic cell. *Nat Med.* 1997;3(7):730-737.
24. Okada S, Nakauchi H, Nagayoshi K, Nishikawa S, Miura Y, Suda T. In vivo and in vitro stem cell function of c-kit- and Sca-1-positive murine hematopoietic cells. *Blood.* 1992;80(12):3044-3050.
25. Singh SK, Hawkins C, Clarke ID, et al. Identification of human brain tumour initiating cells. *Nature.* 2004;432(7015):396-401.
26. O'Brien CA, Pollett A, Gallinger S, Dick JE. A human colon cancer cell capable of initiating tumour growth in immunodeficient mice. *Nature.* 2007;445(7123):106-110.
27. Lee CJ, Dosch J, Simeone DM. Pancreatic cancer stem cells. *J Clin Oncol.* 2008;26(17):2806-2812.
28. Lam WK, Watkins DN. Lung cancer: future directions. *Respirology.* 2007;12(4):471-477.
29. Hadnagy A, Gaboury L, Beaulieu R, Balicki D. SP analysis may be used to identify cancer stem cell populations. *Exp Cell Res.* 2006;312(19):3701-3710.
30. Gibbs CP, Kukekov VG, Reith JD, et al. Stem-like cells in bone sarcomas: implications for tumorigenesis. *Neoplasia.* 2005;7(11):967-976.
31. Atlasi Y, Mowla SJ, Ziaee SA, Bahrami AR. OCT-4, an embryonic stem cell marker, is highly expressed in bladder cancer. *Int J Cancer.* 2007;120(7):1598-1602.
32. Savona M, Talpaz M. Getting to the stem of chronic myeloid leukaemia. *Nat Rev Cancer.* 2008;8(5):341-350.
33. Cox CV, Evely RS, Oakhill A, Pamphilon DH, Goulden NJ, Blair A. Characterization of acute lymphoblastic leukemia progenitor cells. *Blood.* 2004;104(9):2919-2925.
34. Cox CV, Martin HM, Kearns PR, Virgo P, Evely RS, Blair A. Characterization of a progenitor cell population in childhood T-cell acute lymphoblastic leukemia. *Blood.* 2007;109(2):674-682.
35. Plasschaert SL, Kamps WA, Vellenga E, de Vries EG, de Bont ES. Prognosis in childhood and adult acute lymphoblastic leukaemia: a question of maturation? *Cancer Treat Rev.* 2004;30(1):37-51.
36. Kayo H, Yamazaki H, Nishida H, Dang NH, Morimoto C. Stem cell properties and the side population cells as a target for interferon-alpha in adult T-cell leukemia/lymphoma. *Biochem Biophys Res Commun.* 2007;364(4):808-814.
37. Massa S, Balciunaite G, Ceredig R, Rolink AG. Critical role for c-kit (CD117) in T cell lineage commitment and early thymocyte development in vitro. *Eur J Immunol.* 2006;36(3):508-511.
38. Agosti V, Corbacioglu S, Ehlers I, et al. Critical role for Kit-mediated Src kinase but not PI 3-kinase signaling in pro T and pro B cell development. *J Exp Med.* 2004;199(6):867-878.
39. Parrott JA, Kim G, Skinner MK. Expression and action of kit ligand/stem cell factor in normal human and bovine ovarian surface epithelium and ovarian cancer. *Biol Reprod.* 2000;62(6):1600-1609.
40. Stier S, Cheng T, Dombkowski D, Carlesso N, Scadden DT. Notch1 activation increases hematopoietic stem cell self-renewal in vivo and favors lymphoid over myeloid lineage outcome. *Blood.* 2002;99(7):2369-2378.
41. Radtke F, Wilson A, Mancini SJ, MacDonald HR. Notch regulation of lymphocyte development and function. *Nat Immunol.* 2004;5(3):247-253.
42. Weng AP, Ferrando AA, Lee W, et al. Activating mutations of NOTCH1 in human T cell acute lymphoblastic leukemia. *Science.* 2004;306(5694):269-271.
43. Masuda K, Kakugawa K, Nakayama T, Minato N, Katsura Y, Kawamoto H. T cell lineage determination precedes the initiation of TCR beta gene rearrangement. *J Immunol.* 2007;179(6):3699-3706.
44. Tripp A, Liu Y, Sieburg M, Montalbano J, Wrzesinski S, Feuer G. Human T-cell leukemia virus type 1 tax oncoprotein suppression of multilineage hematopoiesis of CD34+ cells in vitro. *J Virol.* 2003;77(22):12152-12164.
45. Miyazaki M, Miyazaki K, Itoi M, et al. Thymocyte proliferation induced by pre-T cell receptor signaling is maintained through polycomb gene product Bmi-1-mediated Cdkn2a repression. *Immunity.* 2008;28(2):231-245.
46. Ishikawa F, Yoshida S, Saito Y, et al. Chemotherapy-resistant human AML stem cells home to and engraft within the bone-marrow endosteal region. *Nat Biotechnol.* 2007;25(11):1315-1321.

Inhibition of the SDF-1α–CXCR4 axis by the CXCR4 antagonist AMD3100 suppresses the migration of cultured cells from ATL patients and murine lymphoblastoid cells from HTLV-I *Tax* transgenic mice

Akira Kawaguchi,[1-3] Yasuko Orba,[1,3] Takashi Kimura,[1] Hidekatsu Iha,[4] Masao Ogata,[5] Takahiro Tsuji,[2] Akira Ainai,[2,6] Tetsutaro Sata,[2] Takashi Okamoto,[7] William W. Hall,[8] Hirofumi Sawa,[1,3] and Hideki Hasegawa[2,6]

[1]Department of Molecular Pathobiology, Research Center for Zoonosis Control, Hokkaido University, Hokkaido, Japan; [2]Department of Pathology, National Institute of Infectious Diseases, Tokyo, Japan; [3]Global COE Program, Hokkaido University, Hokkaido, Japan; [4]Department of Infectious Diseases, Oita University Faculty of Medicine, Oita, Japan; [5]Blood Transfusion Center, Oita University Hospital, Oita, Japan; [6]Center for Influenza Virus Research, National Institute of Infectious Diseases, Tokyo, Japan; [7]Department of Molecular and Cellular Biology, Nagoya City University Graduate School of Medical Sciences, Nagoya City, Japan; and [8]Centre for Research in Infectious Diseases, University College Dublin, Dublin, Ireland

Adult T-cell leukemia (ATL) is a T-cell malignancy caused by human T lymphotropic virus type I, and presents as an aggressive leukemia with characteristic widespread leukemic cell infiltration into visceral organs and skin. The molecular mechanisms associated with leukemic cell infiltration are poorly understood. We have used mouse models of ATL to investigate the role of chemokines in this process. Transfer of splenic lymphomatous cells from transgenic to SCID mice reproduces a leukemia and lymphoma that is histologically identical to human disease. It could be shown that lymphomatous cells exhibit specific chemotactic activity in response to stromal cell–derived factor-1α (SDF-1α). Lymphomatous cells exhibited surface expression of CXCR4, the specific receptor of SDF-1α. AMD3100, a CXCR4 antagonist, was found to inhibit both SDF-1α–induced migration and phosphorylation of extracellular signal-related kinase 1/2. Investigation of cultured cells from human ATL patients revealed identical findings. Using the SCID mouse model, it could be demonstrated that AMD3100 inhibited infiltration of lymphomatous cells into liver and lung tissues in vivo. These results demonstrate the involvement of the SDF-1α/CXCR4 interaction as one mechanism of leukemic cell migration and this may provide a novel target as part of combination therapy for ATL. (Blood. 2009;114: 2961-2968)

Introduction

Adult T-cell leukemia (ATL) is a peripheral T-cell malignancy caused by infection by human T lymphotropic virus type I (HTLV-I). This hematologic neoplasm develops in 1% to 5% of people infected with HTLV-I usually 2 to 4 decades after infection. A characteristic manifestation of ATL is extensive infiltration of leukemic cells into various organs, including lymph nodes, liver, spleen, lungs, and skin.[1,2] Tissue infiltration likely reflects certain unique biologic properties of the leukemic cells, and although these are poorly understood they may be related to the expression and function of chemokines, chemokine receptors,[3-7] adhesion molecules,[8,9] and resulting adhesive interactions with endothelial cells.

Chemokines are a group of structurally related cytokines that induce directed migration of various leukocyte populations.[10] Chemokine receptors are coupled to heterotrimeric G proteins and induce cell movement toward a concentration gradient of the cognate chemokine ligand.[11] Chemokines are essential for the migration and tissue localization of various lymphocyte subpopulations expressing specific chemokine receptors. Human stromal cell–derived factor-1α (SDF-1α), also known as CXCL12, binds and signals solely though chemokine receptor CXCR4.[12] CXCR4 is central to stem cell localization, serving as a chemoattractant for lymphocytes in vitro and in vivo.[13] In addition, a recent study demonstrated that the CXCR4 signal pathway may play a role in the metastasis of breast cancer cells by inducing chemotactic and invasive responses.[14]

Human ATL cells have been shown to produce several chemokines, including macrophage inflammatory protein 1α (MIP-1α),[3] MIP-3α,[4] MIP-1β,[5] I-309,[6] thymus- and activation-regulated chemokine (TARC), and macrophage-derived chemokine (MDC),[7] and express the chemokine receptors CCR4,[15] CCR5,[16] CCR7,[17] and CCR9,[18] and it has been suggested that some of these may be involved in ATL cell migration and infiltration.

Recently, we have established a model of ATL by generating HTLV-I *Tax* transgenic mice with a restriction of transgene expression to developing thymocytes.[19] These mice developed aggressive leukemic and lymphoma with a characteristic histologic phenotype showing extensive perivascular infiltration of leukemia cells into spleen, liver, kidney, lung, lymph nodes, and skin. Flow cytometric analyses demonstrated that the cells were $CD4^-$ and $CD8^-$, but positive for both CD44 and cytoplasmic CD3 indicative of a thymus-derived pre–T-cell phenotype. Cells also expressed high levels of activation markers including CD25. Lymphomatous cells from these transgenic mice could reproduce identical disease after intraperitoneal injection into SCID mice. In this study, we have used the SCID mouse model to investigate molecular mechanisms associated with leukemic cell infiltration, and have focused on the chemotactic activity of the lymphomatous cells. We

Submitted November 12, 2008; accepted June 22, 2009. Prepublished online as *Blood* First Edition paper, August 5, 2009; DOI 10.1182/blood-2008-11-189308.

The online version of this article contains a data supplement.

The publication costs of this article were defrayed in part by page charge payment. Therefore, and solely to indicate this fact, this article is hereby marked "advertisement" in accordance with 18 USC section 1734.

Table 1. Clinical and laboratory characteristics of ATL patients

Case	Date of collection	Age/sex	Subtype at diagnosis	Date of onset	WBC ($\times 10^9$/L)	Atypical cells (%)*	LDH, IU/L (normal range)†	Serum Ca (mM)‡	Infiltrated organs
1	10/16/2007	No data	Chronic	No data	16.8	80	NE	NE	NE
2	6/9/2000	70/F	Chronic	5/22/2000	26.3	34	701 (212-410)	2.20	PB
3	5/3/2003	53/M	Acute	5/3/2003	30.9	69	1426 (212-410)	Normal	PB, S, superficial LN, LN in the abdominal cavity
4	11/17/2004	45/F	Acute	11/17/2004	65.5	83	307 (119-229)	2.65	PB, S, L, Sp
5	5/1/1998	51/M	Acute	2/20/1998	58.8	88	4979 (212-410)	2.53	PB, Sp
6	11/8/1996	36/M	Acute	11/6/1996	37.9	NE	1349 (212-410)	2.29	PB, S, superficial LN, L, Sp

NE indicates not examined; PB, peripheral blood; S, skin; L, liver; Sp, spleen; and LN, lymph nodes.
*Atypical cells were morphologically diagnosed.
†Normal range was changed in 2004.
‡Normal range: 8.2-10.2 mg/dL.

could demonstrate that not only primary murine lymphomatous cells but also human ATL cells exhibit specific chemotactic activity in response to SDF-1α and that this is associated with a specific interaction with CXCR4 and activation of extracellular signal-related kinase 1/2 (ERK1/2) signaling. It could also be shown that AMD3100, a specific CXCR4 antagonist,[20] markedly inhibited cell migration and phosphorylation of ERK1/2 by SDF-1α in both murine and human cells. In addition, AMD3100 inhibited infiltration of lymphomatous cells into liver and lung tissues in SCID mice. These results have identified a novel molecular mechanism associated with leukemic cell migration and provide a framework for designing new therapeutic strategies for the treatment of ATL.

Methods

Cells

Tumor cells from spleens of HTLV-I *Tax*-transgenic mice, in which normal splenocytes were replaced with lymphomatous cells, were isolated using a Lymphoprep kit (Axis-Shield ProC As), and suspended in RPMI 1640 medium. Thereafter, lymphomatous cells (10^6/mL) were intraperitoneally injected into SCID mice. At 28 days after injection, tumor cells were again isolated from ascites and spleens of the injected SCID mice. The isolated tumor cells from SCID mice (primary murine lymphoblastoid [pML] cells) were harvested and kept frozen until use. The pML cells were cultured in RPMI 1640 medium supplemented with 10% fetal bovine serum (FBS; Hyclone), antibiotics, and 2 mM L-glutamine, and maintained at 37°C in 5% CO_2 and investigated after 1 or 2 days in culture. As a control, T cells were isolated from spleens of C57BL/6 mice with a Pan T-cell Isolation Kit (Miltenyi Biotec). Isolated control T cells were cultured in the same conditions as that of pML cells. Leukemic cells from ATL patients who were diagnosed on the basis of characteristic clinical features and laboratory findings were isolated by Ficoll-Hypaque gradient centrifugation and kept frozen until use. The cells were cultured for 2 days in RPMI 1640 medium supplemented with 20% FBS (Equitech-Bio), antibiotics, 2 mM L-glutamine, and 1 ng/mL interleukin-2 (IL-2; Peprotech EC), and maintained at 37°C in 5% CO_2. Isolated cells contained more than 90% leukemic cells at the time of analysis. The clinical and laboratory characteristics of ATL patients are shown in Table 1.

All animal experiments were approved by the Animal Care and Use Committee of the Hokkaido University School of Medicine and the Animal Care and Use Committee of the National Institute of Infectious Diseases. Tumor cells from ATL patients were maintained in RPMI 1640 medium supplemented with 15% FBS (Equitech-Bio), penicillin G (50 U/mL), and streptomycin (50 μg/mL;Sigma-Aldrich). Ethical permission for use of patient-derived cells and pathologic materials was approved by the Ethical Committee of the Oita University Faculty of Medicine and informed consent was obtained in accordance with the Declaration of Helsinki.

Antibodies and chemicals

Antibodies for phosphorylated forms of p44/42 mitogen-activated protein kinase, Akt, p38, phosphatidylinositol 3 kinase (PI3K), and IκB, and total forms of p44/42 mitogen-activated protein kinase, Akt, and IκB were obtained from Cell Signaling Technology. Anti–mouse/human CXC-chemokine receptor 4 (CXCR4/CD184) polyclonal antibody was purchased from eBioscience. Recombinant mouse thymus and activation regulated chemokine (TARC/CCL17), macrophage inflammatory protein 3α (MIP-3α/CCL20), recombinant murine and human stromal cell–derived factor-1α (SDF-1α/CXCL12) were purchased from Peprotech EC. Recombinant murine regulated on activation normal T expressed and secreted (RANTES/CCL5) and cutaneous T cell–attracting chemokine (CTACK/CCL27) were purchased from Acris Antibodies. Recombinant mouse secondary lymphoid-tissue chemokine (SLC/Exodus-2) was purchased from Chemicon International. The CXCR4 antagonist, AMD3100 octahydrochloride, was purchased from Sigma-Aldrich. Mitogen-activated protein kinase (MEK) inhibitor, U0126, was purchased from Promega. All recombinant chemokines and antagonists were dissolved in distilled water, and U0126 was dissolved in dimethyl sulfoxide. For immunohistochemical staining, monoclonal antihuman/mouse CXCL12/SDF-1 antibody (1:100; R&D Systems) was used.

Immunoblotting

pML cells were serum-starved for 2 hours, and then lysates from 10^6 cells per sample were prepared after stimulation with SDF-1α (100 ng/mL) at the indicated time points. Protein content was determined using a Pierce BCA Protein Assay kit. Equal amounts of protein were separated by polyacrylamide gel electrophoresis and transferred onto polyvinylidene difluoride membranes (Immobilon-P; Millipore).

Chemotaxis assay

For cells from both ATL patients and pML cells, the migration efficiency of cells was assessed using 5-μm-pore Transwell filter membranes (Kurabo). For each membrane filter, 5×10^6 cells were cultured in 200 μL RPMI 1640 containing 0.5% bovine albumin. The membrane insert was placed in the well of the 24-well plate that contained 500 μL RPMI medium with murine recombinant chemokine the noted concentrations, and incubated at 37°C for 2.5 hours. After removal of filter inserts, the number of cells that had migrated from the upper chamber to the lower well was counted using a hemocytometer viewed under a microscope. Chemokines used in the assays are as described in "Antibodies and chemicals." To examine the effect of antagonists on SDF-1α–induced chemotactic activity, cells were incubated with antagonists for 1 hour and then loaded in the upper chamber. Migrated cells were counted using a hemocytometer. The effect of SDF-1α on cell survival was measured by assays of viability at 24 or 48 hours.

Flow cytometry

For quantification of cell-surface CXCR4 receptor expression, pML cells were incubated for 30 minutes with PE-conjugated rat anti–mouse-CD184/

CXCR4 monoclonal antibody (× 20; BD Pharmingen), or PE-anti–rat IgG2b (Beckman Coulter) as an isotype control. The data obtained were analyzed using Flowjo software (Tree Star).

Reverse transcription and reverse-transcription–polymerase chain reaction

Total RNA was prepared from pML cells using TRIzol reagent (Gibco-BRL). Total RNA (1 μg) was reverse-transcribed with Omniscript reverse transcriptase (QIAGEN), according to the manufacturer's instructions. Polymerase chain reaction (PCR) was carried out in a volume of 20 μL; initial denaturation at 94°C for 2 minutes was followed by 30 cycles of 94°C for 15 seconds, 58°C for 30 seconds, and 68°C for 30 seconds. As an internal control, *β-actin* was also amplified. The following primers were used: for *Tax*, 5′-AGGCAGATGAGAATGACCATGA-3′ and 5′-TTTTCACTC-CCAGGCTCTAAGC-3′; for SDF-1α, 5′-CACCGATCCACACAGAG-TACTTG-3′ and 5′-AGCCAACGTCAAGCATCTGA-3′; for β-actin, 5′-CTCCTTAATGTCAGCGATTTC-3′ and 5′-CAGCCGTGCAACAA-TCTGAA-3′. PCR products were electrophoresed in agarose gel, and visualized using a UV illuminator.

Immunohistochemistry

Tissues were fixed in neutral-buffered formalin (Sigma-Aldrich), embedded in paraffin, sectioned, and stained with hematoxylin and eosin (H&E). For immunohistochemical staining, the sections were deparaffinized with xylene and dehydrated using decreasing concentrations of ethanol. Thereafter, sections were boiled in a pressure cooker for 2 minutes in 0.01 M citrate buffer (pH 6.0) for antigen retrieval. Mouse sections were incubated with 0.3% H_2O_2 in methanol at room temperature for 15 minutes to block endogenous peroxidase. After washing with PBS, sections were pretreated with blocking solution A (Histofine; Nichirei Biosciences) at room temperature for 60 minutes. The sections were sequentially incubated with primary antibody at 4°C overnight, with blocking solution B (Nichirei Biosciences) for 10 minutes, and with universal immunoperoxidase polymer (Nichirei Biosciences) for 10 minutes. The signal was visualized with diamino-3,3′-diaminobenzidine. For human sections, slides were initially treated with peroxidase block solution (Dako) for 5 minutes, and incubated with 10% normal goat serum (Nichirei Biosciences) at room temperature for 60 minutes. The sections were incubated with primary antibody at 4°C overnight, and thereafter followed by incubation for 90 minutes with labeled polymer-HRP antimouse conjugation (Envision system; Dako) and color development using diamino-3,3′-diaminobenzidine. Tumor cells from human ATL patients were stained by the Giemsa method to confirm their morphology. To examine expression of SDF-1α in human tissues infiltrated by ATL cells, liver samples infiltrated by ATL cells from ATL cases (n = 5) were immunohistochemically examined.

AMD3100 in vivo treatment

SCID mice (6-week-old; nontreated [NT]) were inoculated intraperitoneally with AMD3100 pretreated (AMD^+) or NT pML cells (5×10^2, 5×10^3, and 5×10^4 cells/mice, n = 5 in each group). In AMD^+ group, the pML cells were incubated with 20 μg/mL AMD3100 in RPMI (0.3% fetal calf serum) at 37°C for 30 minutes as described previously.[21] The mice inoculated with AMD^+ pML cells were treated with 300 μg AMD3100 daily for 3 weeks (5 days per week) intraperitoneally (AMD-treated mice). The mice inoculated with NT pML cells were treated with PBS for 3 weeks (5 days per week) intraperitoneally (untreated mice). The mice were killed at 23 days after inoculation of pML cells. Genomic DNA of liver and lung tissues was extracted, and the copy numbers of *Tax* gene and *β-actin* gene were measured by quantitative real-time PCR using QuantiTect Probe PCR Kit (QIAGEN). The relative copy number of *Tax* was represented by the ratio to the copy number of *β-actin* gene. The primers used for detection of *Tax* genome and *β-actin* gene were as follows: Tax forward: 5′-aggcagatgacaat-gaccatga-3′, Tax reverse: 5′-ttttcactcccaggctctaagc-3′, Tax probe: 5′-FAM-ccccaaatatcccccggg-TAMRA-3′, and beta-actin forward: 5′-caccgatccaca-cagagtacttg-3′, β-actin reverse: 5′-cagtgctgtctggtggtacca-3′, and β-actin probe: 5′-FAM-cagtaatctccttctgcatcctgtcagcaa-TAMRA-3′.

Statistics

Statistical comparisons between experimental groups were analyzed using the Student *t* test, and for all comparisons a *P* value less than .05 was considered significant.

Results

Chemotactic response of pML cells to SDF-1α

Several studies have reported that human ATL cells exhibit chemotactic activity in response to the chemokines TARC, SLC, and RANTES.[7,10-12] We examined the chemotactic activity of pML cells in response to several cytokines and chemokines. Specifically, the pML cell migratory response to 6 different chemokines, TARC, MIP-3α, RANTES, SLC, CTACK, and SDF-1α, was investigated using a chemotaxis chamber assay. It could be shown that pML cells had a marked, dose-dependent chemotactic response to SDF-1α (Figure 1A). The cells also showed a weak chemotactic response to TARC and SLC, which has been reported for human ATL cells.[7,10,12] The migratory efficiencies of pML cells and control normal mouse T cells in response to SDF-1α were compared and it could be clearly shown that the migratory response of pML cells was markedly higher (Figure 1B).

We examined the effect of SDF-1α on survival of pML cells. SDF-1α had no effect on survival of pML cells after 24- and 48-hour incubation. We also investigated the effect of NF-κB inhibitor (BAY65-1942), which induces apoptosis of pML cells at

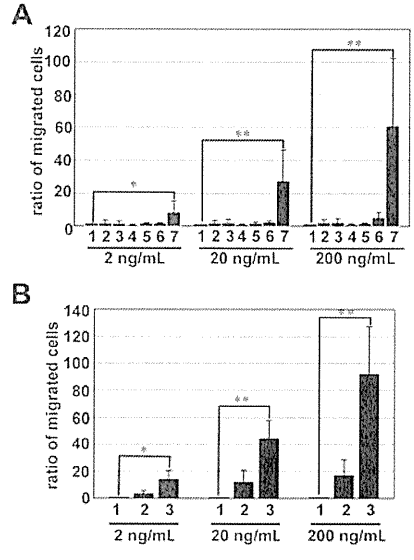

Figure 1. Chemotactic activity of pML cells in response to various chemokines. (A) Chemotactic activity of pML cells in response to chemokines SDF-1α, MIP-3α, TARC, SLC, RANTES, and CTACK. Migration efficiency of pML cells was estimated using a Transwell assay in the presence of various concentrations (2, 20, and 200 ng/mL) of chemokines. The number of migrating pML cells was counted using a hemocytometer viewed under a microscope. The results are expressed as the fold number of the untreated control pML cells. The number below each bar corresponds to each chemokine: 1, control; 2, TARC; 3, LARC; 4, RANTES; 5, CTACK; 6, SLC; and 7, SDF-1α. These results were confirmed by 3 independent experiments. The data are presented as mean values ± SD. $^*P < .05$. $^{**}P < .01$. (B) Chemotactic activity of pML cells and normal T cells. The number of migrating cells was measured as described for panel B in the presence of 0, 2, 20, and 200 ng/mL SDF-1α. The results are expressed as the fold number of the normal T cells. These results were confirmed by 3 independent experiments. The data are presented as mean values ± SD. $^*P < .05$; $^{**}P < .01$.

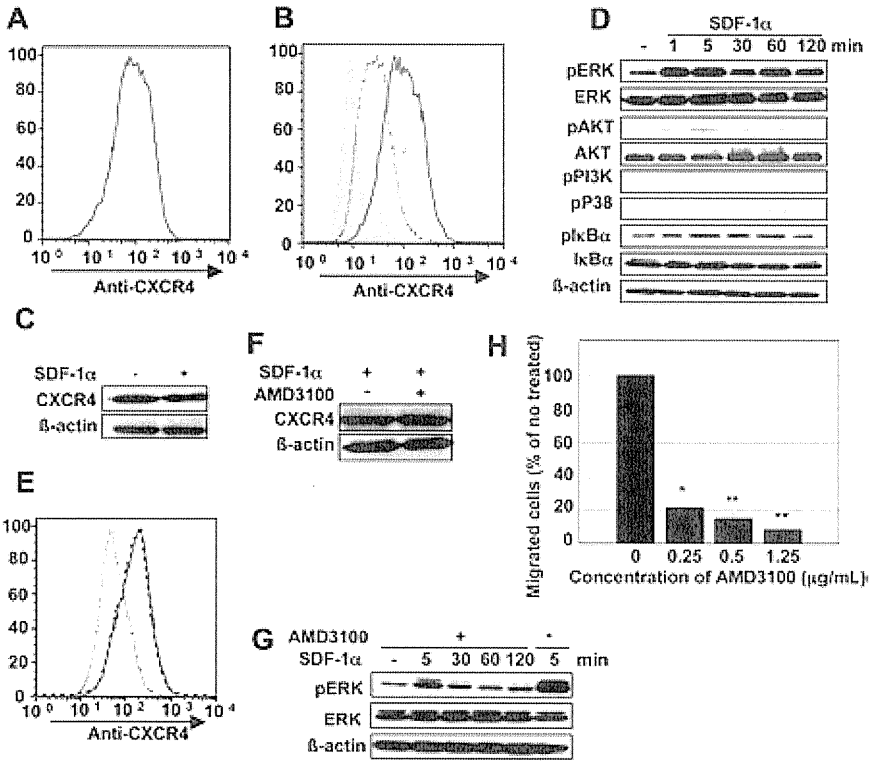

Figure 2. CXCR4 expression on the surface of pML cells and SDF-1α–induced CXCR4 translocation. (A) Flow cytometric analysis of cell-surface expression of CXCR4 in pML cells. CXCR4 was detected by incubating cells with PE-conjugated rat anti-CXCR4 antibody. Red line represents CXCR4 expression, and gray area represents the result of staining with isotype-matched control antibody. (B) CXCR4 expression on pML cell surface. Cells were treated in the presence (blue dot line) or absence (red line) of 100 ng/mL SDF-1α. After a brief wash, cells were incubated with the same antibody as used in Figure 2A. The gray area represents staining with isotype-matched control antibody. (C) Total cellular protein level of CXCR4 in the presence (+) or absence (−) of SDF-1α (100 ng/mL) for 5 minutes. (D) SDF-1α–induced phosphorylation of ERK1/2 in pML cells. pML cells were treated before lysis with 100 ng/mL SDF-1α for the indicated times. Cell lysates were analyzed by immunoblotting analysis with anti–phospho-ERK, –total ERK, –phospho-AKT, –total AKT, –phospho-PI3K, –phospho-P38, –phospho-IκBα, –total IκBα, or –β-actin antibodies. (E) Expression levels of cellular surface CXCR4 in pML cells after treatment with AMD3100. Cells were pretreated with 25 μg/mL AMD3100 for 1 hour, and then stimulated with SDF-1α for 5 minutes (black dot line). Cells were also stimulated exclusively with SDF-1α (blue dot line) or were untreated (red line). The gray area represents staining with isotype-matched control antibody. (F) Expression of total CXCR4 protein with (+) or without (−) AMD3100 treatment. The lysates from treated cells were analyzed by immunoblotting with anti–mouse/human CXCR4 polyclonal antibody. (G) Phosphorylation of ERK1/2 in pML cells with or without AMD3100 treatment. After pretreatment with AMD3100 (25 μg/mL) for 1 hour, cells were stimulated with SDF-1α for the indicated times (0, 5, 30, 60, and 120 minutes). The cellular lysates were analyzed by immunoblotting. In the lane at the right, the cells received no AMD3100 treatment but were stimulated with SDF-1α. (H) Migration assay of pML cells using AMD3100 at various concentrations (0, 0.25, 0.5, and 1.25 μg/mL). pML cells were preincubated for 60 minutes with AMD3100 at the indicated concentrations, and then subjected to the migration assay in the presence of 100 ng/mL SDF-1α. The data were presented as a relative ratio of migrating cells: the number of migrated cells in the presence of AMD3100/the number of nontreated cells. These results were confirmed by 3 independent experiments. The data are presented as mean values ± SD. $*P < .05$. $**P < .01$.

24 hours after incubation, to determine whether SDF-1α might reverse this. More than 80% of the pML cells were dead at 24 hours after incubation with BAY65-1942, and it could be clearly shown that SDF-1α could not reverse the effect of the inhibitor and permit the survival of the pML cells (supplemental Figure 1, available on the *Blood* website; see the Supplemental Materials link at the top of the online article).

Cell surface localization of CXCR4 in pML cells

Flow cytometry analysis was used to examine expression of CXCR4, which is the specific receptor for SDF-1α on pML cells, and it could be shown that CXCR4 was localized on the cell surface (Figure 2A). Chemokine binding to their cell surface receptors is known to lead to internalization of the receptor-ligand complex, with subsequent activation of intracellular signal cascades.[22] To investigate the effect of SDF-1α on CXCR4 expression, we analyzed CXCR4 localization after treatment with SDF-1α (100 ng/mL). It could be demonstrated that treatment with SDF-1α down-regulated CXCR4 surface expression (Figure 2B). Total expression levels of CXCR4 protein were unaffected (Figure 2C), demonstrating that cell surface CXCR4 in pML cells was internalized upon exposure to SDF-1α.

Intracellular signal pathways regulated by SDF-1α/CXCR4 in pML cells

SDF-1α is known to activate the ERK1/2 pathway. ERK1/2 is a downstream effector of the MEK-dependent signaling cascade, and the MEK-ERK pathway is an important mediator of chemotaxis in many cell types.[23,24] To confirm whether SDF-1α treatment activates the MEK-ERK pathway in pML cells, we initially examined phosphorylation of ERK1/2. Immunoblotting with phospho-ERK antibody revealed that SDF-1α treatment led to a rapid activation of ERK1/2 (Figure 2D), with phosphorylation of ERK1/2 evident within 1 minute and peaking at 5 minutes after SDF-1α exposure. This was sustained at least until 120 minutes. No significant changes were observed in total ERK protein expression over this time period (Figure 2D). These results were consistent with a previous study in which SDF-1α was shown to promote internalization of CXCR4 and activation of ERK1/2 in multiple myeloma cells.[25] Phosphorylation of ERK1/2 was found to be abrogated by the MEK inhibitor U0126, even in the presence of SDF-1α (supplemental Figure 2A), and about 40% decrease in the migration of pML cells was observed in chemotaxis assays (supplemental Figure 2B). To further analyze CXCR4/SDF-1α–mediated intracellular signaling, we investigated whether SDF-1α

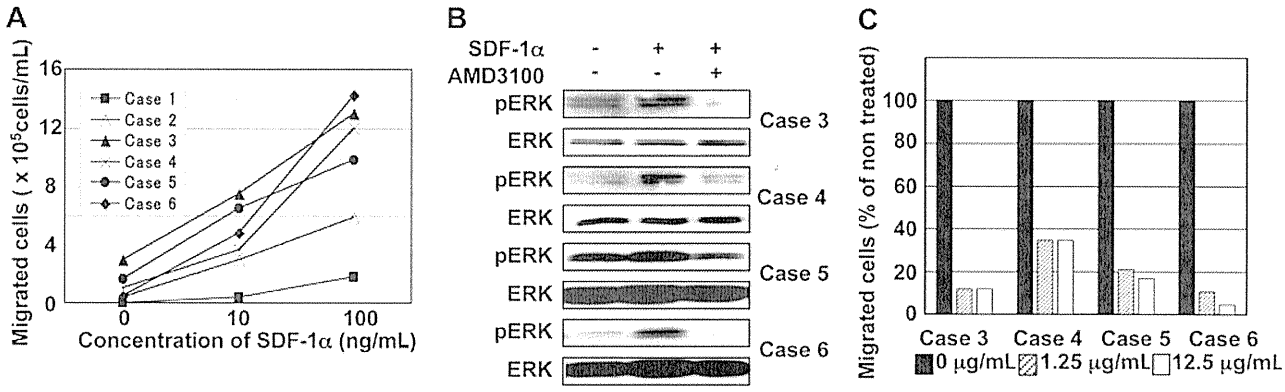

Figure 3. Chemotaxis of human ATL cells in response to SDF-1α. (A) The migration assay of human ATL cells freshly prepared from frozen stocks of ATL patient's peripheral blood mononuclear cells and cultured for 2 days. Human ATL cells were also examined for chemotactic activity in response to SDF-1α, using recombinant human SDF-1α. After incubation with SDF-1α for 2.5 hours, the number of the cells migrating to the lower chamber was counted using a hemocytometer. (B) Phosphorylation of ERK1/2 after stimulation with SDF-1α (100 ng/mL for 5 minutes) in human ATL cells with or without AMD3100 pretreatment (25 μg/mL for 1 hour). (C) The inhibitory effect of AMD3100 on the migration of human ATL cells. Human ATL cells were preincubated for 60 minutes with the indicated concentrations of AMD3100, and then applied to the migration assay in the presence of 100 ng/mL SDF-1α. The number of the migrating cells was counted, and represented in the bar graph as a relative ratio of migrated to nontreated cells.

activated other molecules downstream of CXCR4. In contrast to ERK1/2, phosphorylation of several other molecules, including PI3K, Akt, p38, and IκBα, was not significantly affected (Figure 2D). These results demonstrate that SDF-1α exclusively activates the MEK-ERK pathway in pML cells.

Effects of the CXCR4 antagonist AMD3100 in pML cells

We investigated the effect of the selective CXCR4 antagonist AMD3100 on chemotaxis and ERK1/2 signaling. As previously shown, CXCR4 surface expression was down-regulated by SDF-1α treatment (100 ng/mL); however, this inhibition was abrogated by AMD3100 treatment (25 μg/mL; Figure 2E). Total levels of CXCR4 protein expression were unchanged by AMD3100 treatment (Figure 2F). We also examined whether AMD3100 affects phosphorylation of ERK1/2, and it could be demonstrated that phosphorylation was markedly decreased (Figure 2D,G). SDF-1α–induced migration activity of pML cells was assayed in the presence of AMD3100 and compared with untreated cells, and migration was found to be inhibited 79% and 91.2% in the presence of 0.25 and 1.25 μg/mL AMD3100, respectively (Figure 2H). These results show that AMD3100 inhibits the migration of pML cells in a dose-dependent manner by inhibiting the MEK-ERK pathway downstream of CXCR4-SDF-1α.

Chemotaxis of cells derived from ATL patients in response to SDF-1α

To determine whether the results of our mouse model accurately reflected human disease, we analyzed chemotactic activity of leukemic cells from 6 ATL patients after short-term culture (2 days) in response to SDF-1α. Clinical and laboratory information relating to the patients is summarized in Table 1. Phenotypic analysis of the leukemic cells showed that all cell populations were $CD4^+/CD25^+$, and Giemsa staining clearly demonstrated typical features of ATL with cells having enlarged nuclei, often with lobulation, compared with normal peripheral blood lymphocytes (data not shown). All of the ATL cells exhibited chemotaxis in response to SDF-1α treatment in a dose-dependent manner (Figure 3A). In addition, immunoblotting revealed that SDF-1α–induced phosphorylation of ERK1/2 occurred in 4 of the 6 ATL cases examined (Figure 3B); immunoblotting studies in the 2 remaining cases could not be carried out due to insufficient amounts of cell lysates. AMD3100 treatment of the human ATL cells strongly blocked phosphorylation of ERK1/2 (Figure 3B) and abrogated cell migration (Figure 3C). These results clearly demonstrate involvement of the SDF-1α/CXCR4-ERK pathway in human ATL cell migration, and the inhibitory potential of AMD3100.

SDF-1α expression in tissues

SDF-1α is constitutively expressed in numerous tissues in mice.[26] We confirmed expression of SDF-1α mRNA in various organs, including brain, heart, lung, liver, spleen, and kidney. However, we were unable to demonstrate a positive signal for SDF-1α mRNA expression in pML cells (Figure 4A). To examine the presence of SDF-1α protein, we used 2 different antibodies for tissue analysis, and could detect positive signals using a monoclonal anti-CXCL12/SDF-1 antibody. Weak immunopositive signals for SDF-1α protein were observed in epithelial cells of mouse liver hepatic ducts (Figure 4B-C); no positive signals were observed in control experiments that used normal mouse IgG instead of primary antibody (data not shown). In HTLV-I *Tax* transgenic mice, leukemic cell infiltration was readily observed in areas surrounding the SDF-1α–immunopositive hepatic ducts (Figure 4D-E).

In ATL patients, SDF-1α–immunopositive signals were readily detected in the epithelial cells of hepatic ducts that were surrounded by infiltrating leukemic cells. (Figure 4F-G). We also observed SDF-1α immunostaining in epithelial cells of regenerative hepatic ducts in regions infiltrated by leukemic cells (Figure 4H-I). Infiltrating cells were also detected in the portal triad region, and again specifically around the hepatic ducts where epithelial cells were positive for SDF-1α (Figure 4F-I). We also performed immunostaining with anti–SDF-1α antibody of control disease-free human liver samples, and immunopositive staining was also detected in hepatic duct epithelial cells (Figure 4J-K).

Inhibition of pML cell invasion by AMD3100 in vivo

We performed in vivo experiments to determine whether AMD3100 could inhibit leukemic cell invasion in SCID mice. The mice were inoculated intraperitoneally with AMD3100 pretreated (AMD^+) or nontreated (NT) pML cells (5×10^2, 5×10^3, and 5×10^4 cells/mice, n = 5 in each group). The mice inoculated with AMD^+ pML cells were treated with AMD3100 (AMD-treated mice), and control mice inoculated with NT pML

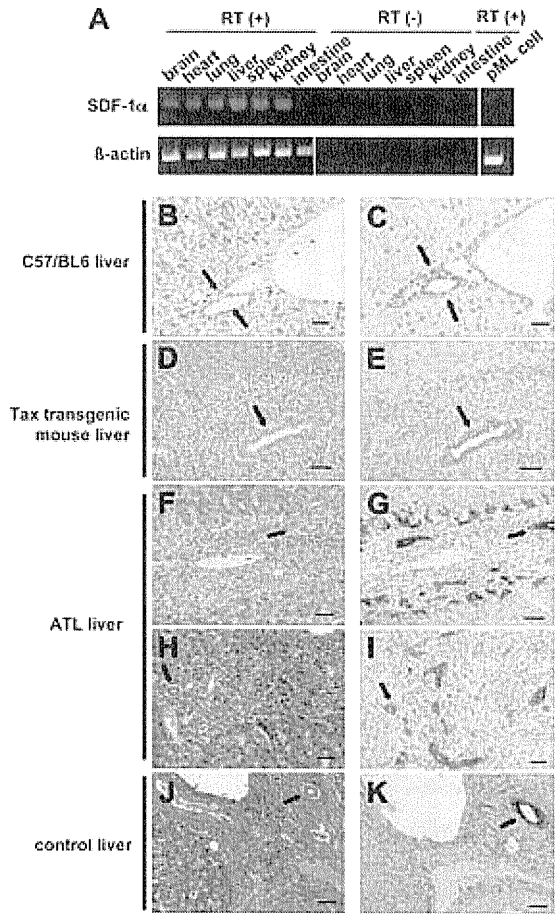

Figure 4. Tissue expression of SDF-1α. (A) The expression levels of SDF-1α transcripts in various tissues of C57BL/6 mice, including brain, heart, lung, liver, spleen, kidney, and intestine with or without reverse transcriptase (RT) reaction. In the lane at the right, the expression level of SDF-1α transcripts in pML cells was also examined. β-Actin was used as an internal control. Vertical lines have been inserted to indicate a repositioned gel lane. (B-K) Immunohistochemical analysis of SDF-1α protein. H&E staining (B,D) and immunostaining (C,E) of SDF-1α in bile ducts from a normal C57BL/6 mouse (B-C) and in a bile duct surrounded by infiltrating tumor cells from a HTLV-I *Tax* transgenic mouse (D-E). Black arrows indicate the same bile duct in serial sections for panels B and C and panels D and E. Bars indicate (B-C) 20 μm or (D-E) 50 μm. Immunohistochemical analysis of SDF-1α protein in liver bile ducts from ATL patients (F-I) and a patient without ATL (J-K). Serial sections of H&E-stained liver from ATL patients (F,H) were examined with immunostaining using anti–SDF-1α antibody (G,I). Black arrows indicate the same bile duct in serial sections for panels F and G and panels H and I. Serial sections of (J) H&E-stained liver from a patient without ATL were also analyzed for (K) SDF-1α expression. Black arrows indicate serial sections of the same bile ducts for panels J and K. Bars indicate 50 μm. Brown indicates immunopositive reaction (C,E,G,I,K).

cells were treated with PBS (untreated mice) for 3 weeks (5 times per week) through intraperitoneal injection. The mice were killed at 23 days after pML cell inoculation. Invasion of pML cells containing the HTLV-I *Tax* gene into liver and lung tissues was examined using quantitative real-time PCR. The relative copy number of *Tax* was represented by the ratio to the copy number of β-actin (Figure 5). In the pML cell–inoculated group (5×10^2), the *Tax* gene was not detected in the liver of either AMD-treated or untreated mice (n = 5 in each group), whereas *Tax* was exclusively detected in one lung tissue of 5 untreated mice (Figure 5). When the mice were inoculated with 5×10^3 pML cells, the ratio of *Tax* genome to *β-actin* gene was significantly inhibited in AMD-treated mice in both liver and lung tissues compared with untreated mice. Furthermore, *Tax* was detected in all of the untreated mice (n = 5), whereas this was not detected in any of the AMD-treated mice (n = 5,

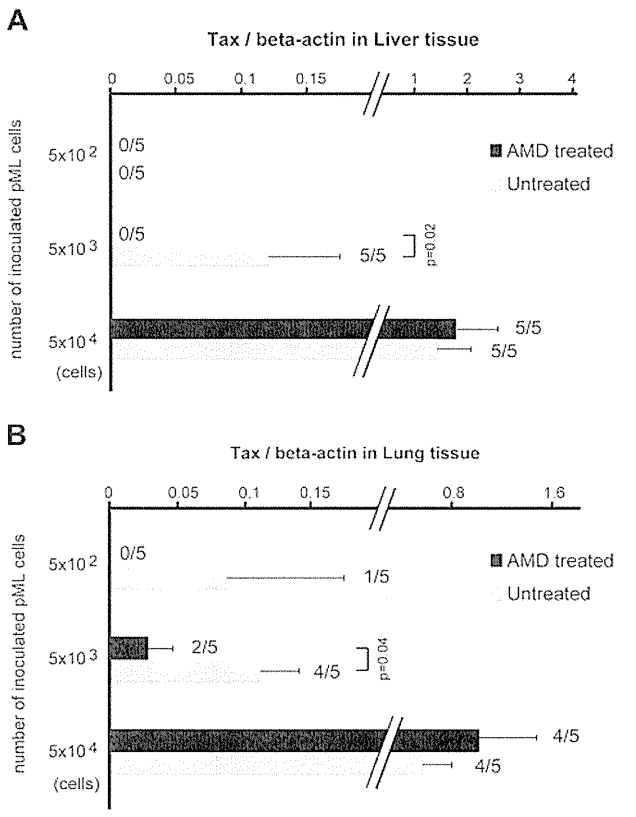

Figure 5. Inhibition of pML cell invasion by AMD3100 in vivo. Infiltration of pML cells to the liver (A) and lung (B) was inhibited by AMD3100 treatment. SCID mice inoculated with pML cells (5×10^2, 5×10^3, and 5×10^4 cells/mice) were treated with either AMD3100 (AMD treated) or PBS (untreated) for 3 weeks (5 times per week) through intraperitoneal injection. Infiltration of pML cells that contain the HTLV-I *Tax* gene into liver and lung tissues was examined using quantitative real-time PCR. The relative copy number of *Tax* genome of the group (inoculated with 5×10^2, 5×10^3, and 5×10^4 pML cells) was represented by the ratio to the copy number of β-actin in liver (A) and lung (B) tissues. The ratio of *Tax*-positive mice/total number of mice was represented on the right side of each bar (mean ± SE).

Figure 5). No significant differences were observed between AMD-treated and untreated mice (n = 5, in each group) that were inoculated with 5×10^4 pML cells (Figure 5). Thus, CXCR4/SDF-1α plays a key role in migration of ATL cells in vivo and AMD3100 inhibits infiltration of pML cells into liver and lung. The results also show that the inhibitory effect of AMD3100 on tissue infiltration of pML cells is influenced by the numbers of inoculated pML cells.

Discussion

Patients with aggressive ATL characteristically display symptoms of leukemic cell infiltration in multiple organs including skin, bone marrow, spleen, liver, lung, and brain. However, the mechanisms of ATL cell infiltration are poorly understood. Chemokines are small secretory proteins that control migration and activation of leukocytes and other types of cells through interaction with a group of 7-transmembrane-domain G protein–coupled receptors (GPCRs). It is known that chemokines may also promote cellular growth and survival and have been associated with metastasis in several malignancies. Specifically it has been shown that breast cancer cells express CXCR4, and high concentrations of SDF-1α are typically present at metastatic sites of breast cancer.[14] The interaction between SDF-1α and CXCR4 has also been implicated in bone metastasis in prostate cancer.[27]

Little is known about the role of G proteins and GPCRs in the life cycle and pathogenesis of HTLV-I. Studies have shown that CCR4[10] and CCR7[2] are frequently expressed in ATL cells, and chemokines, including MCP-1,[3] RANTES,[11] MIP-1α,[5] and SDF-1α,[18,28] have been shown to modulate migration and tissue localization of HTLV-I–infected cells. In addition, expression of the HTLV-I regulatory protein Tax in immortalized T-cell lines has been shown to be involved the activation of the SDF-1α/CXCR4 pathway.[29]

The present study has clearly demonstrated the cell surface expression of CXCR4 on leukemic cells, a specific chemotactic response to SDF-1α, and that cell migration is associated with MEK-ERK signaling. Following the interaction with SDF-1α, surface CXCR4 translocates to an intracellular compartment.[22] It has been demonstrated that the GPCR heteromultimerized with receptors of tyrosine kinases translocated to the endosome and promoted activation of endosomal Ras-ERK pathways in several cell types.[30] Thus, it is possible that the subcellular localization of CXCR4 in pML cells may also promote activation of additional signaling pathways, in addition to ERK1/2, and this is currently under investigation.

Our studies also demonstrated that the CXCR4 antagonist AMD3100 inhibited cell migration in response to SDF-1α. The MEK inhibitor U0126 was found to inhibit the chemotaxis of pML cells and also inhibited phosphorylation of ERK1/2. In contrast, AMD3100 although significantly suppressing the chemotactic activity of pML cells, had less impact on the phosphorylation of ERK1/2 compared with U0126 (Figure 2G-H and supplemental Figure 1). These results suggest that phosphorylation of ERK1/2 may also be regulated by other cellular factors. Indeed, it is likely that other signaling pathways and other processes are involved downstream of CXCR4. We also performed a Mouse Inflammatory Cytokine and Receptors Microarray analysis, in which 113 key genes are involved, to determine the possible role of other chemokine receptors (SABiosciences). Using pML cells and pan T cells derived from B6 mice, we could not observe any up-regulation of other chemokine receptors in pML cells. Thus, although the SDF-1α/CXCR4 pathway appears to be uniquely important, it is almost certain that other pathways also contribute to leukemic cell invasion, including cell adhesion molecules,[8,9] matrix metalloproteinases,[31] and other biomolecules.[32] Microarray data have been deposited to Gene Expression Omnibus (GEO) and can be found under accession numbers GSE17341, GSM433627, and GSM433628.[33]

The results obtained from our previous and the present studies also confirm that our murine models do accurately reproduce human disease in that, in addition to developing the clinical and pathologic features of ATL, we also demonstrated a dose-dependent promotion of chemotactic activity by SDF-1α, phosphorylation of ERK1/2, and an AMD3100 inhibition of SDF-1α–induced ERK1/2 phosphorylation and migration in primary human ATL cells.

SDF-1α is released from fibroblasts and is ubiquitously expressed in many tissues, including liver, kidney, and lung.[26] We confirmed SDF-1α mRNA expression in range of mouse tissues (Figure 4A) and that expression of SDF-1α may be associated with invasion of leukemic cells both in the mouse model and human disease.

AMD3100 is currently being evaluated in a phase 1 trial using healthy volunteers,[34] and in a phase 2 trial involving HIV-I–infected patients.[35] In addition, this drug is considered to be a promising candidate for the treatment of other disorders in which SDF-1α/CXCR4 interactions may be important, including rheumatoid arthritis,[36] breast cancer metastasis,[37] atherosclerosis, and asthma.[38] We demonstrated that AMD3100 inhibited infiltration of pML cells into liver and lung tissues in SCID mice but that the inhibitory effect was influenced by the number of inoculated pML cells. These results imply that when a large number of leukemic cells are used in the inoculation, this can overcome the inhibitory effect of AMD3100. This could be related to the levels of AMD3100, and may require more optimal dosing, or to other unknown factors. This is currently under investigation but our results prove in principle the role of AMD3100 in preventing infiltration of leukemic cells and support the findings of our in vitro experiments. Our studies also suggest that AMD3100 should be a considered as a candidate agent as part of combination therapy of ATL. It has been shown that a combination of α interferon with retrovir can produce significant remission in certain ATL patients,[39] and it is possible that the addition of AMD3100 could contribute to the efficacy of this combination. It is certainly likely that leukemic cell infiltration will involve other molecular mechanisms, and as such combination therapy in the future would also include inhibitors of these processes. Clinical trials in our murine model and ultimately in human disease will ascertain whether CXCR4 antagonists and other agents will play a role and/or contribute to treatment efficacy in combination therapeutic approaches.

Acknowledgments

We thank Ms S. Yamanouchi and Ms M. Sasada for technical assistance, and Drs T. Suzuki and Y. Makino for valuable suggestions.

Y.O. is a research fellow of the Japan Society for the Promotion of Science.

This study was supported in part by grants from the Ministry of Education, Culture, Sports, Science, and Technology; the Ministry of Health, Labor, and Welfare, Japan; the Japan Health Sciences Foundation; the Naito Foundation; the Takeda Science Foundation; and the Program of Founding Research Centers for Emerging and Reemerging Infectious Diseases, MEXT, Japan.

Authorship

Contribution: A.K., T.K., H.S., and H.H. designed research; H.H., H.S., and W.W.H. developed the ATL animal model; A.K., Y.O., and A.A. performed research; H.I., M.O., and T.O. contributed new reagents/materials; T.T. and T.S. contributed pathologic analysis; and A.K., W.W.H., H.S., and H.H. wrote the paper.

Conflict-of-interest disclosure: The authors declare no competing financial interests.

Correspondence: Hideki Hasegawa, Department of Pathology, National Institute of Infectious Diseases, 4-7-1 Gakuen, Musashimurayama City, Tokyo, Japan, 208-0011; e-mail: hasegawa@nih.go.jp; or Hirofumi Sawa, Department of Molecular Pathobiology, Research Center for Zoonosis Control, Hokkaido University, Sapporo, N20, W10, Kita-ku, Sapporo, Japan, 001-0020; e-mail: h-sawa@czc.hokudai.ac.jp.

References

1. Uchiyama T. Human T cell leukemia virus type I (HTLV-I) and human diseases. *Annu Rev Immunol.* 1997;15:15-37.
2. Matsuoka M. Human T-cell leukemia virus type I and adult T-cell leukemia. *Oncogene.* 2003; 22(33):5131-5140.
3. Mori N, Ueda A, Ikeda S, et al. Human T-cell leukemia virus type I tax activates transcription of the human monocyte chemoattractant protein-1

gene through two nuclear factor-kappaB sites. *Cancer Res.* 2000;60(17):4939-4945.

4. Imaizumi Y, Sugita S, Yamamoto K, et al. Human T cell leukemia virus type-I Tax activates human macrophage inflammatory protein-3 alpha/CCL20 gene transcription via the NF-kappa B pathway. *Int Immunol.* 2002;14(2):147-155.
5. Tanaka Y, Mine S, Figdor CG, et al. Constitutive chemokine production results in activation of leukocyte function-associated antigen-1 on adult T-cell leukemia cells. *Blood.* 1998;91(10):3909-3919.
6. Ruckes T, Saul D, Van Snick J, Hermine O, Grassmann R. Autocrine antiapoptotic stimulation of cultured adult T-cell leukemia cells by overexpression of the chemokine I-309. *Blood.* 2001; 98(4):1150-1159.
7. Shimauchi T, Imai S, Hino R, Tokura Y. Production of thymus and activation-regulated chemokine and macrophage-derived chemokine by CCR4+ adult T-cell leukemia cells. *Clin Cancer Res.* 2005;11(6):2427-2435.
8. Ishikawa T, Imura A, Tanaka K, Shirane H, Okuma M, Uchiyama T. E-selectin and vascular cell adhesion molecule-1 mediate adult T-cell leukemia cell adhesion to endothelial cells. *Blood.* 1993;82(5):1590-1598.
9. Tatewaki M, Yamaguchi K, Matsuoka M, et al. Constitutive overexpression of the L-selectin gene in fresh leukemic cells of adult T-cell leukemia that can be transactivated by human T-cell lymphotropic virus type 1 Tax. *Blood.* 1995;86(8): 3109-3117.
10. Campbell DJ, Kim CH, Butcher EC. Chemokines in the systemic organization of immunity. *Immunol Rev.* 2003;195:58-71.
11. Yoshie O, Imai T, Nomiyama H. Chemokines in immunity. *Adv Immunol.* 2001;78:57-110.
12. Nagasawa T, Nakajima T, Tachibana K, et al. Molecular cloning and characterization of a murine pre-B-cell growth-stimulating factor/stromal cell-derived factor 1 receptor, a murine homolog of the human immunodeficiency virus 1 entry coreceptor fusin. *Proc Natl Acad Sci U S A.* 1996; 93(25):14726-14729.
13. Bleul CC, Fuhlbrigge RC, Casasnovas JM, Aiuti A, Springer TA. A highly efficacious lymphocyte chemoattractant, stromal cell-derived factor 1 (SDF-1). *J Exp Med.* 1996;184(3):1101-1109.
14. Lee BC, Lee TH, Avraham S, Avraham HK. Involvement of the chemokine receptor CXCR4 and its ligand stromal cell-derived factor 1alpha in breast cancer cell migration through human brain microvascular endothelial cells. *Mol Cancer Res.* 2004;2(6):327-338.
15. Yoshie O, Fujisawa R, Nakayama T, et al. Frequent expression of CCR4 in adult T-cell leukemia and human T-cell leukemia virus type 1-transformed T cells. *Blood.* 2002;99(5):1505-1511.
16. Mori N, Krensky AM, Ohshima K, et al. Elevated expression of CCL5/RANTES in adult T-cell leukemia cells: possible transactivation of the CCL5 gene by human T-cell leukemia virus type I tax. *Int J Cancer.* 2004;111(4):548-557.
17. Hasegawa H, Nomura T, Kohno M, et al. Increased chemokine receptor CCR7/EBI1 expression enhances the infiltration of lymphoid organs by adult T-cell leukemia cells. *Blood.* 2000;95(1): 30-38.
18. Nagakubo D, Jin Z, Hieshima K, et al. Expression of CCR9 in HTLV-1+ T cells and ATL cells expressing Tax. *Int J Cancer.* 2007;120(7):1591-1597.
19. Hasegawa H, Sawa H, Lewis MJ, et al. Thymus-derived leukemia-lymphoma in mice transgenic for the Tax gene of human T-lymphotropic virus type I. *Nat Med.* 2006;12(4):466-472.
20. Hatse S, Princen K, Bridger G, De Clercq E, Schols D. Chemokine receptor inhibition by AMD3100 is strictly confined to CXCR4. *FEBS Lett.* 2002;527(1-3):255-262.
21. Colmone A, Amorim M, Pontier AL, Wang S, Jablonski E, Sipkins DA. Leukemic cells create bone marrow niches that disrupt the behavior of normal hematopoietic progenitor cells. *Science.* 2008;322(5909):1861-1865.
22. Neel NF, Schutyser E, Sai J, Fan GH, Richmond A. Chemokine receptor internalization and intracellular trafficking. *Cytokine Growth Factor Rev.* 2005;16(6):637-658.
23. Ganju RK, Brubaker SA, Meyer J, et al. The alpha-chemokine, stromal cell-derived factor-1alpha, binds to the transmembrane G-protein-coupled CXCR-4 receptor and activates multiple signal transduction pathways. *J Biol Chem.* 1998;273(36):23169-23175.
24. Peng SB, Peek V, Zhai Y, et al. Akt activation, but not extracellular signal-regulated kinase activation, is required for SDF-1alpha/CXCR4-mediated migration of epitheloid carcinoma cells. *Mol Cancer Res.* 2005;3(4):227-236.
25. Alsayed Y, Ngo H, Runnels J, et al. Mechanisms of regulation of CXCR4/SDF-1 (CXCL12)-dependent migration and homing in multiple myeloma. *Blood.* 2007;109(7):2708-2717.
26. Tashiro K, Tada H, Heilker R, Shirozu M, Nakano T, Honjo T. Signal sequence trap: a cloning strategy for secreted proteins and type I membrane proteins. *Science.* 1993;261(5121):600-603.
27. Kukreja P, Abdel-Mageed AB, Mondal D, Liu K, Agrawal KC. Up-regulation of CXCR4 expression in PC-3 cells by stromal-derived factor-1alpha (CXCL12) increases endothelial adhesion and transendothelial migration: role of MEK/ERK signaling pathway-dependent NF-kappaB activation. *Cancer Res.* 2005;65(21):9891-9898.
28. Moriuchi M, Moriuchi H, Fauci AS. HTLV type I Tax activation of the CXCR4 promoter by association with nuclear respiratory factor 1. *AIDS Res Hum Retroviruses.* 1999;15(9):821-827.
29. Twizere JC, Springael JY, Boxus M, et al. Human T-cell leukemia virus type-1 Tax oncoprotein regulates G-protein signaling. *Blood.* 2007; 109(3):1051-1060.
30. Mor A, Philips MR. Compartmentalized Ras/MAPK signaling. *Annu Rev Immunol.* 2006;24: 771-800.
31. Mori N, Sato H, Hayashibara T, et al. Human T-cell leukemia virus type I Tax transactivates the matrix metalloproteinase-9 gene: potential role in mediating adult T-cell leukemia invasiveness. *Blood.* 2002;99(4):1341-1349.
32. Hayashibara T, Yamada Y, Miyanishi T, et al. Vascular endothelial growth factor and cellular chemotaxis: a possible autocrine pathway in adult T-cell leukemia cell invasion. *Clin Cancer Res.* 2001;7(9):2719-2726.
33. National Center for Biotechnology Information. Gene Expression Omnibus (GEO). http://www.ncbi.nlm.nih.gov/geo. Accessed July 28, 2009.
34. Hendrix CW, Flexner C, MacFarland RT, et al. Pharmacokinetics and safety of AMD-3100, a novel antagonist of the CXCR-4 chemokine receptor, in human volunteers. *Antimicrob Agents Chemother.* 2000;44(6):1667-1673.
35. Hendrix CW, Collier AC, Lederman MM, et al. Safety, pharmacokinetics, and antiviral activity of AMD3100, a selective CXCR4 receptor inhibitor, in HIV-1 infection. *J Acquir Immune Defic Syndr.* 2004;37(2):1253-1262.
36. Nanki T, Hayashida K, El-Gabalawy HS, et al. Stromal cell-derived factor-1-CXC chemokine receptor 4 interactions play a central role in CD4+ T cell accumulation in rheumatoid arthritis synovium. *J Immunol.* 2000;165(11):6590-6598.
37. Müller A, Homey B, Soto H, et al. Involvement of chemokine receptors in breast cancer metastasis. *Nature.* 2001;410(6824):50-56.
38. Abi-Younes S, Sauty A, Mach F, Sukhova GK, Libby P, Luster AD. The stromal cell-derived factor-1 chemokine is a potent platelet agonist highly expressed in atherosclerotic plaques. *Circ Res.* 2000;86(2):131-138.
39. Bazarbachi A, Nasr R, El-Sabban ME, et al. Evidence against a direct cytotoxic effect of alpha interferon and zidovudine in HTLV-I associated adult T cell leukemia/lymphoma. *Leukemia.* 2000; 14(4):716-721.

Vol 459|4 June 2009|doi:10.1038/nature07969

LETTERS

Frequent inactivation of A20 in B-cell lymphomas

Motohiro Kato[1,2], Masashi Sanada[1,5], Itaru Kato[6], Yasuharu Sato[7], Junko Takita[1,2,3], Kengo Takeuchi[8], Akira Niwa[6], Yuyan Chen[1,2], Kumi Nakazaki[1,4,5], Junko Nomoto[9], Yoshitaka Asakura[9], Satsuki Muto[1], Azusa Tamura[1], Mitsuru Iio[1], Yoshiki Akatsuka[11], Yasuhide Hayashi[12], Hiraku Mori[13], Takashi Igarashi[2], Mineo Kurokawa[4], Shigeru Chiba[3], Shigeo Mori[14], Yuichi Ishikawa[8], Koji Okamoto[10], Kensei Tobinai[9], Hitoshi Nakagama[10], Tatsutoshi Nakahata[6], Tadashi Yoshino[7], Yukio Kobayashi[9] & Seishi Ogawa[1,5]

A20 is a negative regulator of the NF-κB pathway and was initially identified as being rapidly induced after tumour-necrosis factor-α stimulation[1]. It has a pivotal role in regulation of the immune response and prevents excessive activation of NF-κB in response to a variety of external stimuli[2–7]; recent genetic studies have disclosed putative associations of polymorphic *A20* (also called *TNFAIP3*) alleles with autoimmune disease risk[8,9]. However, the involvement of A20 in the development of human cancers is unknown. Here we show, using a genome-wide analysis of genetic lesions in 238 B-cell lymphomas, that *A20* is a common genetic target in B-lineage lymphomas. A20 is frequently inactivated by somatic mutations and/or deletions in mucosa-associated tissue lymphoma (18 out of 87; 21.8%) and Hodgkin's lymphoma of nodular sclerosis histology (5 out of 15; 33.3%), and, to a lesser extent, in other B-lineage lymphomas. When re-expressed in a lymphoma-derived cell line with no functional *A20* alleles, wild-type A20, but not mutant A20, resulted in suppression of cell growth and induction of apoptosis, accompanied by downregulation of NF-κB activation. The A20-deficient cells stably generated tumours in immunodeficient mice, whereas the tumorigenicity was effectively suppressed by re-expression of A20. In A20-deficient cells, suppression of both cell growth and NF-κB activity due to re-expression of A20 depended, at least partly, on cell-surface-receptor signalling, including the tumour-necrosis factor receptor. Considering the physiological function of A20 in the negative modulation of NF-κB activation induced by multiple upstream stimuli, our findings indicate that uncontrolled signalling of NF-κB caused by loss of A20 function is involved in the pathogenesis of subsets of B-lineage lymphomas.

Malignant lymphomas of B-cell lineages are mature lymphoid neoplasms that arise from various lymphoid tissues[10,11]. To obtain a comprehensive registry of genetic lesions in B-lineage lymphomas, we performed a single nucleotide polymorphism (SNP) array analysis of 238 primary B-cell lymphoma specimens of different histologies, including 64 samples of diffuse large B-cell lymphomas (DLBCLs), 52 follicular lymphomas, 35 mantle cell lymphomas (MCLs), and 87 mucosa-associated tissue (MALT) lymphomas (Supplementary Table 1). Three Hodgkin's-lymphoma-derived cell lines were also analysed. Interrogating more than 250,000 SNP sites, this platform permitted the identification of copy number changes at an average resolution of less than 12 kilobases (kb). The use of large numbers of SNP-specific probes is a unique feature of this platform, and combined with the CNAG/AsCNAR software, enabled accurate determination of 'allele-specific' copy numbers, and thus allowed for sensitive detection of loss of heterozygosity (LOH) even without apparent copy-number reduction, in the presence of up to 70–80% normal cell contamination[12,13].

Lymphoma genomes underwent a wide range of genetic changes, including numerical chromosomal abnormalities and segmental gains and losses of chromosomal material (Supplementary Fig. 1), as well as copy-number-neutral LOH, or uniparental disomy (Supplementary Fig. 2). Each histology type had a unique genomic signature, indicating a distinctive underlying molecular pathogenesis for different histology types (Fig. 1a and Supplementary Fig. 3). On the basis of the genomic signatures, the initial pathological diagnosis of MCL was re-evaluated and corrected to DLBCL in two cases. Although most copy number changes involved large chromosomal segments, a number of regions showed focal gains and deletions, accelerating identification of their candidate gene targets. After excluding known copy number variations, we identified 46 loci showing focal gains (19 loci) or deletions (27 loci) (Supplementary Tables 2 and 3 and Supplementary Fig. 4).

Genetic lesions on the NF-κB pathway were common in B-cell lymphomas and found in approximately 40% of the cases (Supplementary Table 1), underpinning the importance of aberrant NF-κB activation in lymphomagenesis[11,14] in a genome-wide fashion. They included focal gain/amplification at the *REL* locus (16.4%) (Fig. 1b) and *TRAF6* locus (5.9%), as well as focal deletions at the *PTEN* locus (5.5%) (Supplementary Figs 1 and 4). However, the most striking finding was the common deletion at 6q23.3 involving a 143-kb segment. It exclusively contained the *A20* gene (also called *TNFAIP3*), a negative regulator of NF-κB activation[3–7,15] (Fig. 1b), which was previously reported as a candidate target of 6q23 deletions in ocular lymphoma[16]. LOH involving the *A20* locus was found in 50 cases, of which 12 showed homozygous deletions as determined by the loss of both alleles in an allele-specific copy number analysis (Fig. 1b, Table 1 and Supplementary Table 4). On the basis of this finding, we searched for possible tumour-specific mutations of *A20* by genomic DNA sequencing of entire coding exons of the gene in the same series of lymphoma samples (Supplementary Fig. 5). Because two out of the three Hodgkin's-lymphoma-derived cell lines had biallelic *A20* deletions/mutations (Supplementary Fig. 6), 24 primary samples from Hodgkin's lymphoma were also analysed for mutations, where

[1]Cancer Genomics Project, Department of [2]Pediatrics, [3]Cell Therapy and Transplantation Medicine, and [4]Hematology and Oncology, Graduate School of Medicine, University of Tokyo, 7-3-1 Hongo, Bunkyo-ku, Tokyo 113-8655, Japan. [5]Core Research for Evolutional Science and Technology, Japan Science and Technology Agency, 4-1-8, Honcho, Kawaguchi-shi, Saitama 332-0012, Japan. [6]Department of Pediatrics, Graduate School of Medicine, Kyoto University, 54 Kawahara-cho, Shogoin, Sakyo-ku, Kyoto 606-8507, Japan. [7]Department of Pathology, Okayama University Graduate School of Medicine, Dentistry and Pharmaceutical Sciences, 2-5-1 Shikata-cho, Kita-ku, Okayama 700-8558, Japan. [8]Division of Pathology, The Cancer Institute of Japanese Foundation for Cancer Research, Japan, 3-10-6 Ariake, Koto-ku, Tokyo 135-8550, Japan. [9]Hematology Division, Hospital, and [10]Early Oncogenesis Research Project, Research Institute, National Cancer Center, 5-1-1 Tsukiji, Chuo-ku, Tokyo 104-0045, Japan. [11]Division of Immunology, Aichi Cancer Center Research Institute, 1-1 Kanokoden, Chikusa-ku, Nagoya 464-8681, Japan. [12]Gunma Children's Medical Center, 779 Shimohakoda, Hokkitsu-machi, Shibukawa 377-8577, Japan. [13]Division of Hematology, Internal Medicine, Showa University Fujigaoka Hospital, 1-30, Fujigaoka, Aoba-ku, Yokohama-shi, Kanagawa 227-8501, Japan. [14]Department of Pathology, Teikyo University School of Medicine, 2-11-1 Kaga, Itabashi-ku, Tokyo 173-8605, Japan.

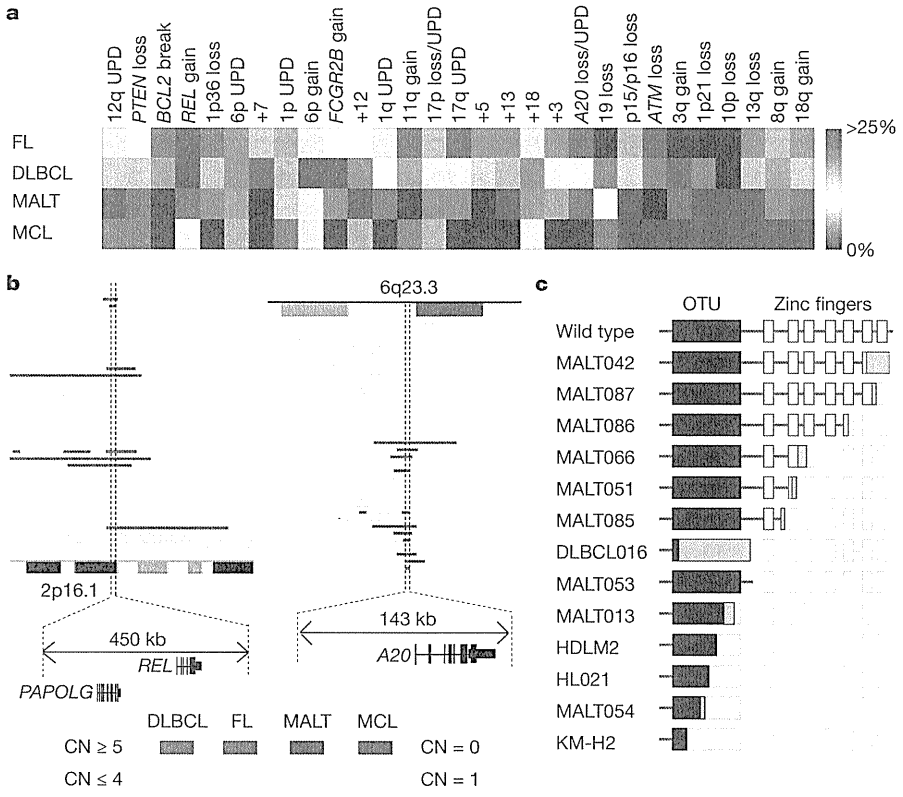

Figure 1 | Genomic signatures of different B-cell lymphomas and common genetic lesions at 2p16-15 and 6q23.3 involving NF-κB pathway genes. **a**, Twenty-nine genetic lesions were found in more than 10% in at least one histology and used for clustering four distinct histology types of B-lineage lymphomas. The frequency of each genetic lesion in each histology type is colour-coded. FL, follicular lymphoma; UPD, uniparental disomy. **b**, Recurrent genetic changes are depicted based on CNAG output of the SNP array analysis of 238 B-lineage lymphoma samples, which include gains at the *REL* locus on 2p16-15 (left panel) and the *A20* locus on 6q23.3 (right panel). Regions showing copy number gain or loss are indicated by horizontal lines. Four histology types are indicated by different colours, where high-grade amplifications and homozygous deletions are shown by darker shades to discriminate from simple gains (copy number ≤4) and losses (copy number = 1) (lighter shades). **c**, Point mutations and small nucleotide insertions and deletions in the *A20* (*TNFAIP3*) gene caused premature truncation of A20 in most cases. Altered amino acids caused by frame shifts are indicated by green bars.

genomic DNA was extracted from 150 microdissected CD30-positive tumour cells (Reed–Sternberg cells) for each sample. *A20* mutations were found in 18 out of 265 lymphoma samples (6.8%) (Table 1), among which 13 mutations, including nonsense mutations (3 cases), frame-shift insertions/deletions (9 cases), and a splicing donor site mutation (1 case) were thought to result in premature termination of translation (Fig. 1c). Four missense mutations and one intronic mutation were identified in five microdissected Hodgkin's lymphoma samples. They were not found in the surrounding normal tissues, and thus, were considered as tumour-specific somatic changes.

In total, biallelic *A20* lesions were found in 31 out of 265 lymphoma samples including 3 Hodgkin's lymphoma cell lines. Quantitative analysis of SNP array data suggested that these *A20* lesions were present in the major tumour fraction within the samples (Supplementary Fig. 7). Inactivation of *A20* was most frequent in MALT lymphoma (18 out of 87) and Hodgkin's lymphoma (7 out of 27), although it was also found in DLBCL (5 out of 64) and follicular lymphoma (1 out of 52) at lower frequencies. In MALT lymphoma, biallelic *A20* lesions were confirmed in 18 out of 24 cases (75.0%) with LOH involving the 6q23.3 segment (Supplementary Fig. 8). Considering the limitation in detecting very small homozygous deletions, *A20* was thought to be the target of 6q23 LOH in MALT lymphoma. On the other hand, the 6q23 LOHs in other histology types tended to be extended into more centromeric regions and less frequently accompanied biallelic *A20* lesions (Supplementary Fig. 8 and Supplementary Table 4), indicating that they might be more heterogeneous with regard to their gene targets. We were unable to analyse Hodgkin's lymphoma samples using SNP arrays owing to insufficient genomic DNA obtained from microdissected samples, and were likely to underestimate the frequency of *A20* inactivation in Hodgkin's lymphoma because we might fail to detect a substantial proportion of cases with homozygous deletions, which explained 50% (12 out of 24) of *A20* inactivation in other histology types. *A20* mutations in Hodgkin's lymphoma were exclusively found in nodular sclerosis classical Hodgkin's lymphoma (5 out of 15) but not in other histology types (0 out of 9), although the possible association requires further confirmation in additional cases.

A20 is a key regulator of NF-κB signalling, negatively modulating NF-κB activation through a wide variety of cell surface receptors and viral proteins, including tumour-necrosis factor (TNF) receptors, toll-like receptors, CD40, as well as Epstein–Barr-virus-associated LMP1 protein[2,5,17,18]. To investigate the role of A20 inactivation in lymphomagenesis, we re-expressed wild-type A20 under a *Tet*-inducible promoter in a lymphoma-derived cell line (KM-H2) that had no functional *A20* alleles (Supplementary Fig. 6), and examined the effect of A20 re-expression on cell proliferation, survival and downstream NF-κB signalling pathways. As shown in Fig. 2a–c and Supplementary Fig. 9, re-expression of wild-type A20 resulted in the suppression of cell proliferation and enhanced apoptosis, and in the concomitant accumulation of IκBβ and IκBε, and downregulation of NF-κB activity. In contrast, re-expression of two lymphoma-derived A20 mutants, $A20^{532Stop}$ or $A20^{750Stop}$, failed to show growth suppression, induction of apoptosis, accumulation of IκBβ and IκBε or downregulation of

Table 1 | Inactivation of A20 in B-lineage lymphomas

Histology	Tissue	Sample	Allele	Uniparental disomy	Exon	Mutation	Biallelic inactivation
DLBCL							5 out of 64 (7.8%)
	Lymph node	DLBCL008	−/−	No	–	–	
	Lymph node	DLBCL016	+/−	No	Ex2	329insA	
	Lymph node	DLBCL022	−/−	No	–	–	
	Lymph node	DLBCL028	−/−	Yes	–	–	
	Lymph node	MCL008*	−/−	Yes	–	–	
Follicular lymphoma							1 out of 52 (1.9%)
	Lymph node	FL024	−/−	No	–	–	
MCL							0 out of 35 (0%)
MALT							18 out of 87 (21.8%)
Stomach							3 out of 23 (13.0%)
	Gastric mucosa	MALT013	+/+	Yes	Ex5	705insG	
	Gastric mucosa	MALT014	+/+	Yes	Ex3	Ex3 donor site>A	
	Gastric mucosa	MALT036	+/−	No	Ex7	delintron6-Ex7†	
Eye							13 out of 43 (30.2%)
	Ocular adnexa	MALT008	−/−	No	–	–	
	Ocular adnexa	MALT017	−/−	No	–	–	
	Ocular adnexa	MALT051	+/−	No	Ex7	1943delTG	
	Ocular adnexa	MALT053	+/+	Yes	Ex6	1016G>A(stop)	
	Ocular adnexa	MALT054	+/−	No	Ex3	502delTC	
	Ocular adnexa	MALT055	−/−	No	–	–	
	Ocular adnexa	MALT066	+/−	No	Ex7	1581insA	
	Ocular adnexa	MALT067	−/−	No	–	–	
	Ocular adnexa	MALT082	−/−	Yes	–	–	
	Ocular adnexa	MALT084	−/−	Yes	–	–	
	Ocular adnexa	MALT085	+/+	Yes	Ex7	1435insG	
	Ocular adnexa	MALT086	+/+	Yes	Ex6	878C>T(stop)	
	Ocular adnexa	MALT087	+/+	Yes	Ex9	2304delGG	
Lung							2 out of 12 (16.7%)
	Lung	MALT042	−/−	No	–	–	
	Lung	MALT047	+/+	Yes	Ex9	2281insT	
Other‡							0 out of 9 (0%)
Hodgkin's lymphoma							7 out of 27 (26.0%)
NSHL	Lymph node	HL10	ND	ND	Ex7	1777G>A(V571I)	
NSHL	Lymph node	HL12	ND	ND	Ex7	1156A>G(R364G)	
NSHL	Lymph node	HL21	ND	ND	Ex4	569G>A(stop)	
NSHL	Lymph node	HL24	ND	ND	Ex3	1487C>A(T474N)	
NSHL	Lymph node	HL23	ND	ND	–	Intron 3§	
	Cell line	KM-H2	−/−	No	–		
	Cell line	HDLM2	+/−	No	Ex4	616ins29bp‖	
Total							31 out of 265 (11.7%)

DLBCL, diffuse large B-cell lymphoma; MALT, MALT lymphoma; MCL, mantle cell lymphoma; ND, not determined because SNP array analysis was not performed; NSHL, nodular sclerosis classical Hodgkin's lymphoma.
* Diagnosis was changed based on the genomic data, which was confirmed by re-examination of pathology.
† Deletion including the boundary of intron 6 and exon 7 (see also Supplementary Fig. 5b).
‡ Including 1 parotid gland, 1 salivary gland, 2 colon and 5 thyroid cases.
§ Insertion of CTC at −19 bases from the beginning of exon 3.
‖ Insertion of TGGCTTCCACAGACACACCCATGGCCCGA.

NF-κB activity (Fig. 2a–c), indicating that these were actually loss-of-function mutations. To investigate the role of A20 inactivation in lymphomagenesis *in vivo*, *A20*- and mock-transduced KM-H2 cells were transplanted in NOD/SCID/γ_c^{null} (NOG) mice[19], and their tumour formation status was examined for 5 weeks with or without induction of wild-type A20 by tetracycline administration. As shown in Fig. 2d, mock-transduced cells developed tumours at the injected sites, whereas the *Tet*-inducible *A20*-transduced cells generated tumours only in the absence of A20 induction (Supplementary Table 5), further supporting the tumour suppressor role of A20 in lymphoma development.

Given the mode of negative regulation of NF-κB signalling, we next investigated the origins of NF-κB activity that was deregulated by A20 loss in KM-H2 cells. The conditioned medium prepared from a 48-h serum-free KM-H2 culture had increased NF-κB upregulatory activity compared with fresh serum-free medium, which was inhibited by re-expression of A20 (Fig. 3a). KM-H2 cells secreted two known ligands for TNF receptor—TNF-α and lymphotoxin-α (Supplementary Fig. 10)[20]—and adding neutralizing antibodies against these cytokines into cultures significantly suppressed their cell growth and NF-κB activity without affecting the levels of their overall suppression after A20 induction (Fig. 3b, d). In addition, recombinant TNF-α and/or lymphotoxin-α added to fresh serum-free medium promoted cell growth and NF-κB activation in KM-H2 culture, which were again suppressed by re-expression of A20 (Fig. 3c, e). Although our data in Fig. 3 also show the presence of factors other than TNF-α and lymphotoxin-α in the KM-H2-conditioned medium—as well as some intrinsic pathways in the cell (Fig. 3a)—that were responsible for the A20-dependent NF-κB activation, these results indicate that both cell growth and NF-κB activity that were upregulated by A20 inactivation depend at least partly on the upstream stimuli that evoked the NF-κB-activating signals.

Aberrant activation of the NF-κB pathway is a hallmark of several subtypes of B-lineage lymphomas, including Hodgkin's lymphoma, MALT lymphoma, and a subset of DLBCL, as well as other lymphoid neoplasms[11,14], where a number of genetic alterations of NF-κB signalling pathway genes[21–25], as well as some viral proteins[26,27], have been implicated in the aberrant activation of the NF-κB pathway[14]. Thus, frequent inactivation of A20 in Hodgkin's lymphoma and MALT and other lymphomas provides a novel insight into the molecular pathogenesis of these subtypes of B-lineage lymphomas through deregulated NF-κB activation. Because A20 provides a

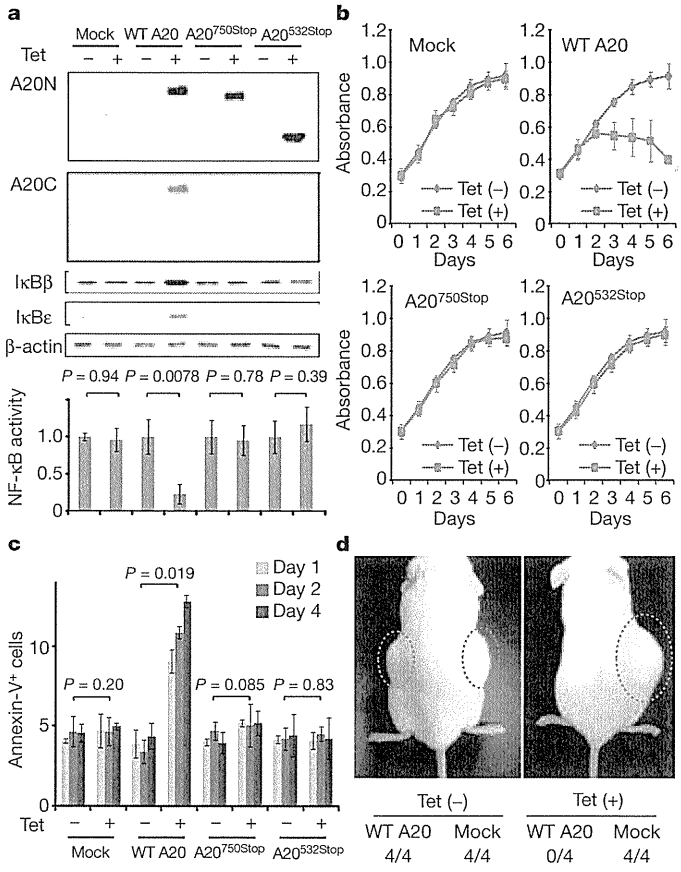

Figure 2 | Effects of wild-type and mutant A20 re-expressed in a lymphoma cell line that lacks the normal *A20* gene. a, Western blot analyses of wild-type (WT) and mutant ($A20^{532Stop}$ and $A20^{750Stop}$) A20, as well as IκBβ and IκBε, in KM-H2 cells, in the presence or absence of tetracycline treatment (top panels). A20N and A20C are polyclonal antisera raised against N-terminal and C-terminal A20 peptides, respectively. β-actin blots are provided as a control. NF-κB activities are expressed as mean absorbance ± s.d. ($n = 6$) in luciferase assays (bottom panel). **b**, Proliferation of KM-H2 cells stably transduced with plasmids for mock and *Tet*-inducible wild-type A20, $A20^{532Stop}$ and $A20^{750Stop}$ was measured using a cell counting kit in the presence (red lines) or absence (blue lines) of tetracycline. Mean absorbance ± s.d. ($n = 5$) is plotted. **c**, The fractions of Annexin-V-positive KM-H2 cells transduced with various *Tet*-inducible A20 constructs were measured by flow cytometry after tetracycline treatment and the mean values (±s.d., $n = 3$) are plotted. **d**, *In vivo* tumorigenicity was assayed by inoculating 7×10^6 KM-H2 cells transduced with mock or *Tet*-inducible wild-type A20 in NOG mice, with (right panel) or without (left panel) tetracycline administration.

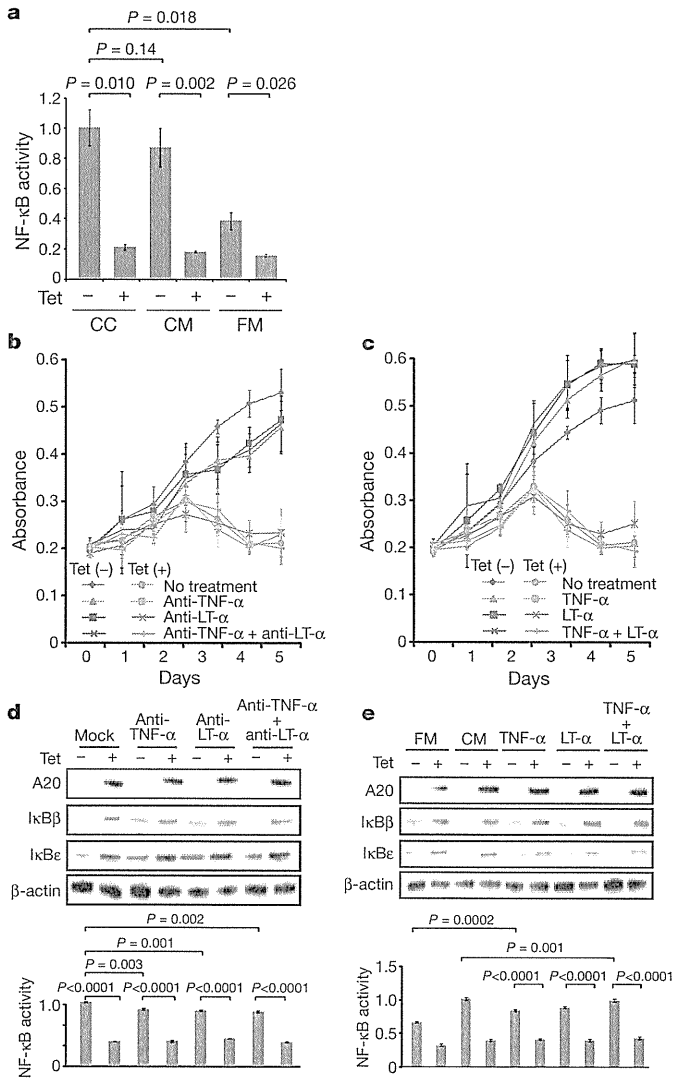

Figure 3 | Tumour suppressor role of A20 under external stimuli. a, NF-κB activity in KM-H2 cells was measured 30 min after cells were inoculated into fresh medium (FM) or KM-H2-conditioned medium (CM) obtained from the 48-h culture of KM-H2, and was compared with the activity after 48 h continuous culture of KM-H2 (CC). A20 was induced 12 h before inoculation in Tet (+) groups. **b, c**, Effects of neutralizing antibodies against TNF-α and lymphotoxin-α (LTα) (**b**) and of recombinant TNF-α and LT-α added to the culture (**c**) on cell growth were evaluated in the presence (Tet (+)) or absence (Tet (−)) of A20 induction. Cell numbers were measured using a cell counting kit and are plotted as their mean absorbance ± s.d. ($n = 6$). **d, e**, Effects of the neutralizing antibodies (**d**) and the recombinant cytokines added to the culture (**e**) on NF-κB activities and the levels of IκBβ and IκBε after 48 h culture with (Tet (+)) or without (Tet (−)) tetracycline treatment. NF-κB activities are expressed as mean absorbance ± s.d. ($n = 6$) in luciferase assays.

negative feedback mechanism in the regulation of NF-κB signalling pathways upon a variety of stimuli, aberrant activation of NF-κB will be a logical consequence of A20 inactivation. However, there is also the possibility that the aberrant NF-κB activity of A20-inactivated lymphoma cells is derived from upstream stimuli, which may be from the cellular environment. In this context, it is intriguing that MALT lymphoma usually arises at the site of chronic inflammation caused by infection or autoimmune disorders and may show spontaneous regression after eradication of infectious organisms[28]; furthermore, Hodgkin's lymphoma frequently shows deregulated cytokine production from Reed–Sternberg cells and/or surrounding reactive cells[29]. Detailed characterization of the NF-κB pathway regulated by A20 in both normal and neoplastic B lymphocytes will promote our understanding of the precise roles of A20 inactivation in the pathogenesis of these lymphoma types. Our finding underscores the importance of genome-wide approaches in the identification of genetic targets in human cancers.

METHODS SUMMARY

Genomic DNA from 238 patients with non-Hodgkin's lymphoma and three Hodgkin's-lymphoma-derived cell lines was analysed using GeneChip SNP genotyping microarrays (Affymetrix). This study was approved by the ethics boards of the University of Tokyo, National Cancer Institute Hospital, Okayama University, and the Cancer Institute of the Japanese Foundation of Cancer Research. After appropriate normalization of mean array intensities, signal ratios between tumours and anonymous normal references were calculated in an allele-specific manner, and allele-specific copy numbers were inferred from the observed signal ratios based on the hidden Markov model using CNAG/AsCNAR software (http://www.genome.umin.jp). *A20* mutations were examined by directly sequencing genomic DNA using a set of primers (Supplementary Table 6). Full-length cDNAs of wild-type and mutant *A20* were introduced into a

lentivirus vector, pLenti4/TO/V5-DEST (Invitrogen), with a *Tet*-inducible promoter. Viral stocks were prepared by transfecting the vector plasmids into 293FT cells (Invitrogen) using the calcium phosphate method and then infected to the KM-H2 cell line. Proliferation of KM-H2 cells was measured using a Cell Counting Kit (Dojindo). Western blot analyses and luciferase assays were performed as previously described. NF-κB activity was measured by luciferase assays in KM-H2 cells stably transduced with a reporter plasmid having an NF-κB response element, pGL4.32 (Promega). Apoptosis of KM-H2 upon A20 induction was evaluated by counting Annexin-V-positive cells by flow cytometry. For *in vivo* tumorigenicity assays, 7×10^6 KM-H2 cells were transduced with the *Tet*-inducible *A20* gene and those with a mock vector were inoculated on the contralateral sides in eight NOG mice[19] and examined for their tumour formation with ($n = 4$) or without ($n = 4$) tetracycline administration. Full copy number data of the 238 lymphoma samples will be accessible from the Gene Expression Omnibus (GEO, http://ncbi.nlm.nih.gov/geo/) with the accession number GSE12906.

Full Methods and any associated references are available in the online version of the paper at www.nature.com/nature.

Received 17 September 2008; accepted 3 March 2009.
Published online 3 May 2009.

1. Dixit, V. M. *et al.* Tumor necrosis factor-α induction of novel gene products in human endothelial cells including a macrophage-specific chemotaxin. *J. Biol. Chem.* **265**, 2973–2978 (1990).
2. Song, H. Y., Rothe, M. & Goeddel, D. V. The tumor necrosis factor-inducible zinc finger protein A20 interacts with TRAF1/TRAF2 and inhibits NF-κB activation. *Proc. Natl Acad. Sci. USA* **93**, 6721–6725 (1996).
3. Lee, E. G. *et al.* Failure to regulate TNF-induced NF-κB and cell death responses in A20-deficient mice. *Science* **289**, 2350–2354 (2000).
4. Boone, D. L. *et al.* The ubiquitin-modifying enzyme A20 is required for termination of Toll-like receptor responses. *Nature Immunol.* **5**, 1052–1060 (2004).
5. Wang, Y. Y., Li, L., Han, K. J., Zhai, Z. & Shu, H. B. A20 is a potent inhibitor of TLR3- and Sendai virus-induced activation of NF-κB and ISRE and IFN-β promoter. *FEBS Lett.* **576**, 86–90 (2004).
6. Wertz, I. E. *et al.* De-ubiquitination and ubiquitin ligase domains of A20 downregulate NF-κB signalling. *Nature* **430**, 694–699 (2004).
7. Heyninck, K. & Beyaert, R. A20 inhibits NF-κB activation by dual ubiquitin-editing functions. *Trends Biochem. Sci.* **30**, 1–4 (2005).
8. Graham, R. R. *et al.* Genetic variants near *TNFAIP3* on 6q23 are associated with systemic lupus erythematosus. *Nature Genet.* **40**, 1059–1061 (2008).
9. Musone, S. L. *et al.* Multiple polymorphisms in the *TNFAIP3* region are independently associated with systemic lupus erythematosus. *Nature Genet.* **40**, 1062–1064 (2008).
10. Jaffe, E. S., Harris, N. L., Stein, H. & Vardiman, J. W. *World Health Organization Classification of Tumours. Pathology and Genetics of Tumours of Hematopoietic and Lymphoid Tissues* (IARC Press, 2001).
11. Klein, U. & Dalla-Favera, R. Germinal centres: role in B-cell physiology and malignancy. *Nature Rev. Immunol.* **8**, 22–33 (2008).
12. Nannya, Y. *et al.* A robust algorithm for copy number detection using high-density oligonucleotide single nucleotide polymorphism genotyping arrays. *Cancer Res.* **65**, 6071–6079 (2005).
13. Yamamoto, G. *et al.* Highly sensitive method for genomewide detection of allelic composition in nonpaired, primary tumor specimens by use of affymetrix single-nucleotide-polymorphism genotyping microarrays. *Am. J. Hum. Genet.* **81**, 114–126 (2007).
14. Jost, P. J. & Ruland, J. Aberrant NF-κB signaling in lymphoma: mechanisms, consequences, and therapeutic implications. *Blood* **109**, 2700–2707 (2007).
15. Durkop, H., Hirsch, B., Hahn, C., Foss, H. D. & Stein, H. Differential expression and function of A20 and TRAF1 in Hodgkin lymphoma and anaplastic large cell lymphoma and their induction by CD30 stimulation. *J. Pathol.* **200**, 229–239 (2003).
16. Honma, K. *et al. TNFAIP3* is the target gene of chromosome band 6q23.3-q24.1 loss in ocular adnexal marginal zone B cell lymphoma. *Genes Chromosom. Cancer* **47**, 1–7 (2008).
17. Sarma, V. *et al.* Activation of the B-cell surface receptor CD40 induces A20, a novel zinc finger protein that inhibits apoptosis. *J. Biol. Chem.* **270**, 12343–12346 (1995).
18. Fries, K. L., Miller, W. E. & Raab-Traub, N. The A20 protein interacts with the Epstein-Barr virus latent membrane protein 1 (LMP1) and alters the LMP1/TRAF1/TRADD complex. *Virology* **264**, 159–166 (1999).
19. Hiramatsu, H. *et al.* Complete reconstitution of human lymphocytes from cord blood $CD34^+$ cells using the NOD/SCID/γ^{null} mice model. *Blood* **102**, 873–880 (2003).
20. Hsu, P. L. & Hsu, S. M. Production of tumor necrosis factor-α and lymphotoxin by cells of Hodgkin's neoplastic cell lines HDLM-1 and KM-H2. *Am. J. Pathol.* **135**, 735–745 (1989).
21. Dierlamm, J. *et al.* The apoptosis inhibitor gene *API2* and a novel 18q gene, *MLT*, are recurrently rearranged in the t(11;18)(q21;q21) associated with mucosa-associated lymphoid tissue lymphomas. *Blood* **93**, 3601–3609 (1999).
22. Willis, T. G. *et al.* Bcl10 is involved in t(1;14)(p22;q32) of MALT B cell lymphoma and mutated in multiple tumor types. *Cell* **96**, 35–45 (1999).
23. Joos, S. *et al.* Classical Hodgkin lymphoma is characterized by recurrent copy number gains of the short arm of chromosome 2. *Blood* **99**, 1381–1387 (2002).
24. Martin-Subero, J. I. *et al.* Recurrent involvement of the *REL* and *BCL11A* loci in classical Hodgkin lymphoma. *Blood* **99**, 1474–1477 (2002).
25. Lenz, G. *et al.* Oncogenic *CARD11* mutations in human diffuse large B cell lymphoma. *Science* **319**, 1676–1679 (2008).
26. Deacon, E. M. *et al.* Epstein-Barr virus and Hodgkin's disease: transcriptional analysis of virus latency in the malignant cells. *J. Exp. Med.* **177**, 339–349 (1993).
27. Yin, M. J. *et al.* HTLV-I Tax protein binds to MEKK1 to stimulate IκB kinase activity and NF-κB activation. *Cell* **93**, 875–884 (1998).
28. Isaacson, P. G. & Du, M. Q. MALT lymphoma: from morphology to molecules. *Nature Rev. Cancer* **4**, 644–653 (2004).
29. Skinnider, B. F. & Mak, T. W. The role of cytokines in classical Hodgkin lymphoma. *Blood* **99**, 4283–4297 (2002).

Supplementary Information is linked to the online version of the paper at www.nature.com/nature.

Acknowledgements This work was supported by the Core Research for Evolutional Science and Technology, Japan Science and Technology Agency, by the 21st century centre of excellence program 'Study on diseases caused by environment/genome interactions', and by Grant-in-Aids from the Ministry of Education, Culture, Sports, Science and Technology of Japan and from the Ministry of Health, Labor and Welfare of Japan for the 3rd-term Comprehensive 10-year Strategy for Cancer Control. We also thank Y. Ogino, E. Matsui and M. Matsumura for their technical assistance.

Author Contributions M.Ka., K.N. and M.S. performed microarray experiments and subsequent data analyses. M.Ka., Y.C., K.Ta., J.T., J.N., M.I., A.T. and Y.K. performed mutation analysis of *A20*. M.Ka., S.Mu., M.S., Y.C. and Y.Ak. conducted functional assays of mutant A20. Y.S., K.Ta., Y.As., H.M., M.Ku., S.Mo., S.C., Y.K., K.To. and Y.I. prepared tumour specimens. I.K., K.O., A.N., H.N. and T.N. conducted *in vivo* tumorigenicity experiments in NOG/SCID mice. T.I., Y.H., T.Y., Y.K. and S.O. designed overall studies, and S.O. wrote the manuscript. All authors discussed the results and commented on the manuscript.

Author Information The copy number data as well as the raw microarray data will be accessible from the GEO (http://ncbi.nlm.nih.gov/geo/) with the accession number GSE12906. Reprints and permissions information is available at www.nature.com/reprints. Correspondence and requests for materials should be addressed to S.O. (sogawa-tky@umin.ac.jp) or Y.K. (ykkobaya@ncc.go.jp).